ADSORPTION OF AS(V), AS(III) AND METHYL ARSENIC BY CALCITE AND THE IMPACT OF SOME GROUNDWATER SPECIES

A Thesis

by

ROBERT GARRET JONES

Submitted to the Office of Graduate Studies of
Texas A&M University
in partial fulfillment of the requirements for the degree of

MASTER OF SCIENCE

May 2007

Major Subject: Soil Science

ADSORPTION OF AS(V), AS(III) AND METHYL ARSENIC BY CALCITE AND THE IMPACT OF SOME GROUNDWATER SPECIES

A Thesis

by

ROBERT GARRET JONES

Submitted to the Office of Graduate Studies of
Texas A&M University
in partial fulfillment of the requirements for the degree of

MASTER OF SCIENCE

Approved by:

Chair of Committee,	Richard H. Loeppert
Committee Members,	Bruce E. Herbert
	Charles T. Hallmark
Head of Department,	David D. Baltensperger

May 2007

Major Subject: Soil Science

ABSTRACT

Adsorption of As(V), As(III) and Methyl Arsenic by Calcite and the

Impact of Some Groundwater Species.

(May 2007)

Robert Garret Jones, B.S., Texas A&M University

Chair of Advisory Committee: Dr. Richard H. Loeppert

The objective of this research was to investigate the retention of arsenate (iAs^{V}), arsenite (iAs^{III}), monomethyl arsenate ($MMAs^{V}$) and dimethyl arsenate ($DMAs^{V}$) by calcite and assess the impact of dissolved Ca^{2+}, Mg^{2+}, phosphate and sulfate on arsenic solubility, adsorption and precipitation phenomena.

Adsorption kinetics of iAs^{V}, evaluated at a low and high concentration, was a relatively rapid process, with a fast initial reaction rate within the first few minutes and a subsequent slower reaction rate as equilibrium was approached. The relative adsorption of arsenicals decreased in the following order: $iAs^{V} > iAs^{III} > DMA^{V} > MMA^{V}$. In no case was a clear adsorption maximum observed with increasing dissolved arsenic concentration. Dissolved 0.01 M Ca^{2+} resulted in an increase in iAs^{V} adsorption; however, in the presence of 0.1 M Ca^{2+} adsorption of iAs^{V} was decreased. The presence of Mg^{2+} as 0.01 M $Mg(NO_3)_2$ resulted in decreased iAs^{V} adsorption probably the result of a lower iAs^{V} affinity for adsorbed Mg^{2+} as compared to Ca^{2+}. Phosphate and sulfate were highly competitive with iAs^{V} in adsorption to calcite and both resulted in decreased iAs^{V} adsorption. The total prevention of iAs^{V} adsorption at initial equimolar arsenic/phosphate concentrations > 88 µM each could be from the consumption of available calcite surface

sites by the specific adsorption of phosphate. Equilibrium modeling, using the geochemical and mineral speciation of equilibrium model (MINTEQA2), indicated that at low concentrations of arsenate or phosphate solid-phase precipitation was not likely and adsorption processes likely controlled solubility. At high concentrations of arsenate $Ca_3(AsO_4)_2 \cdot 3\,{}^2/_3\,H_2O$ and $Ca_3(AsO_4)_2 \cdot 4\,{}^1/_4\,H_2O$ solid phases could be controlling arsenate solubility.

This study indicates that arsenic adsorption response by calcite was different than that of phosphate suggesting that arsenic may not be specifically adsorbed to calcium at the calcite surface. Reduction and biomethylation of arsenic decreased adsorption, suggesting that processes which could affect the speciation of arsenic in the environment, could increase arsenic mobility in environmental systems where calcite and dissolved aqueous calcium play a predominant role in controlling arsenic solubility. Dissolved aqueous concentrations of magnesium, phosphate and sulfate generally reduced the ability of arsenic to be adsorbed to calcite.

ACKNOWLEDGMENTS

I would like to express gratitude for all who have supported me with this educational endeavor. I would like to thank Dr. Wayne Smith and the Department of Soil and Crop Sciences for the assistance I have received throughout my tenure as a graduate student. I would especially like to thank my major advisor, Dr. Richard Loeppert, who has provided me with exceptional guidance throughout this process. I am also thankful for the education and mentorship I have received from Dr. Tom Hallmark and Dr. Bruce Herbert. Thanks, also, to Dr. Dennis James at the Texas A&M University, Center for Chemical Characterization and Analysis for his support throughout many hours of research and analysis. I would also like to acknowledge the Texas Water Resource Institute for providing me with the 2005-2006 W. C. Mills Fellowship.

To all my family and friends, thank you for all your encouragement and support throughout this process and for helping to keep me focused on the more important aspects of life. I would like to give special thanks to my mother for her continued selflessness and sacrifice, which in so many ways has provided me with a wonderful life and made me the person that I am. Finally, I would like to thank my beautiful wife for her bountiful and unwavering love and for her firm dedication to my success and achievement.

TABLE OF CONTENTS

Page

LIST OF TABLES

Page

LIST OF FIGURES

Page

Page

Page

INTRODUCTION

Sedimentary carbonates form by chemical, biological and detrital processes that occur at the ocean floor. Carbonates, in a marine environment, are predominantly created from biogenic processes and their formation depends greatly on biological activity (Ham and Pray, 1962). These sediments are composed principally of skeletal remnants, calcareous excrement of marine organisms and microbially-mediated, lime mud. Depositional and diagenetic processes acting on these sediments over time form carbonate rocks. Carbonate rock classifications are based on depositional texture and porosity, sedimentary structure, fabric, and biological composition (Dunham, 1962; Choquette and Pray, 1970; Embry and Klovan, 1971). Calcite can be a major component of the chemical and mineralogical matrix of the sedimentary, carbonate rock that is formed. Calcite ($CaCO_3$) is the second most abundant mineral at the Earth's surface next to quartz. Calcite in soil can be derived from parent material, from transport processes of water, wind or ice deposition, or from pedogenic processes of dissolution and precipitation which can translocate carbonate minerals spatially within the soil profile. Calcite derived from parent material can be distinguished from pedogenic calcite since it usually exists as larger, sand-size crystals, compared to pedogenic calcite of typically smaller, silt-sized crystals (Doner and Lynn, 1989). The different types of carbonate minerals in soils are classified based on differences in particle size, morphology and crystal arrangement (Doner and Grossl, 2002). Calcite particles are termed micrite, microspar or spar, with sizes of < 5 μm, $5 – 20$ μm and > 20 μm, respectively. Particle

---

This thesis follows the style of Soil Science Society of America Journal.

size affects the reactivity of calcite since a larger reactive surface area to volume ratio occurs as the size of the particles become smaller. Soils which have the characteristic of calcite abundance are known as calcareous soils, and the calcite within these soils can be present as cemented layers, nodules, coatings or particles. Calcareous soils typically occur in arid or semi-arid regions due to the lack of rainfall which limits the weathering and removal of carbonates from the soil profile.

Carbonate minerals tend to exert a dominant effect on the chemistry of soil and groundwater when at a relative abundance of 1% or greater (Langmuir, 1997). Calcite solubility is directly related to pH, soluble Ca activity and the partial pressure of carbon dioxide. The chemical equilibrium in a $CaCO_3$-H_2O-CO_2 system that relates the pH to the partial pressure of CO_2 (P_{CO2}) and calcium activity (Ca^{2+}) is expressed by equation [1],

$$pH = 4.84 - 0.5 \log (Ca^{2+}) - 0.5 \log P_{CO2(g)} \quad [1]$$

adapted from Doner and Grossl (2002). Thus, variability in the partial pressure of CO_2 (P_{CO2}) or Ca^{2+} activity directly affects the solution pH correspondingly. Gaseous carbon dioxide is dissolved into solution and undergoes phase transition to form carbonic acid ($H_2CO_3^o$), which dissociates into hydrogen ion (H^+) and bicarbonate ion (HCO_3^-). As P_{CO2} is increased, additional hydrogen ions are introduced into solution and lower the solution pH when at a fixed Ca^{2+} activity. Conversely, less P_{CO2} causes an increase in the pH of solution when at a fixed Ca^{2+} activity.

The surface of calcite has variable charge character and can be highly reactive due to surface charge development (Mishra, 1978). The electrochemical property at which

the net charge is zero is called the iso-electric point or zero point of charge (ZPC). The pH of the ZPC (pH_{zpc}) for calcite in a $CaCO_3$-H_2O-CO_2 system has been shown by Mishra (1978) to be near the equilibrium pH of 8.2 when at standard atmospheric pressure of CO_2 ($10^{-3.5}$ bar) and room temperature (20^o C). The surface properties and characteristics of calcite change when the pH is different than the pH_{zpc}. A surface complexation model for the calcite-water interface has been proposed by Van Cappellen et al. (1993) and is based on their kinetic studies and the previous X-ray photoelectron spectroscopy study by Stipp and Hochella (1991). The Van Cappellen model suggests that there are specific calcite surface species that are influenced by solution variables such as pH, calcium activity and partial pressure of carbon dioxide. The surface reactions and stability constants for the $CaCO_3$-H_2O-CO_2 system model are represented in Table 1.

Table 1. Surface reactions and stability constants of calcite.

Surface reaction	Log K (25^oC, 1 atm and I = 0)
$>CaOH_2^+ \Leftrightarrow >CaOH^o + H^+$	-12.2
$>CaOH^o \Leftrightarrow >CaO^- + H^+$	-17
$>CaOH^o + CO_2 \Leftrightarrow >CaHCO_3^o$	6.0
$>CaOH^o + CO_2 \Leftrightarrow >CaCO_3^- + H^+$	-2.6
$>CO_3H^o \Leftrightarrow >CO_3^- + H^+$	-4.9
$>CO_3H^o + Ca^{2+} \Leftrightarrow >CO_3Ca^+ + H^+$	-2.8

Adapted from Van Cappellen et al., 1993. Note: The symbol (>) represents the calcite crystal surface.

While this surface complexation model explains surface speciation based on kinetics experiments, it does not incorporate spectroscopic evidence which could directly detect all the surface species that are capable of existing in the $CaCO_3$-H_2O-CO_2 system. Quantitation of calcite-water interface structures under various conditions for the $CaCO_3$-

H_2O-CO_2 system has been performed using high-resolution X-ray reflectivity (Fenter et al., 1999). The calculated abundance of surface species using their best-fit reflectivity model of calcite under experimental conditions at pH 6.8 ($pH < pH_{zpc}$), 8.3 ($pH \sim pH_{zpc}$) and 12.1 ($pH > pH_{zpc}$) for both the calcium and carbonate reaction sites is represented in

Table 2. Surface speciation of calcite.†

pH	log P_{CO2} (atm)	$>CaOH_2^+$	$>CaHCO_3^o$	$>CaCO_3^-$	$>CaOH^o$	$>CO_3^{2-}$	$>CO_3Ca^+$	$>CO_3H^o$
6.83	-3.03	0.970	0.022	0.002	<0.001	0.874	0.128	0.002
8.25	-3.35	0.946	0.034	0.010	<0.001	0.972	0.038	<0.001
12.10	-9.92	0.810	<0.001	0.012	0.178	0.972	0.026	<0.001

† (Fenter et al., 1999.)
‡ The symbol (>) represents the calcite crystal surface

Table 2 (Fenter et al., 1999) and is denoted by a mole proportion based on a total of 2 moles of surface sites. This study indicates that the positively charged calcium-hydroxyl species ($>CaOH_2^+$) is predominant below the pH_{zpc} and that the negatively charged surface-carbonate species ($>CO_3^{2-}$) is predominant above the pH_{zpc}. It has also been indicated in this study that the speciation of calcite as measured by X-ray reflectivity is specific to the terrace sites of the crystal structure and are not indicative of the speciation at defect sites. The defect sites on the calcite crystal surface have much less surface area and are far less abundant than the terrace sites, although it has been suggested that step-edge and kink sites (defect sites) could be primarily responsible for the surface control of complexation reactions that lead to calcite growth and dissolution (Paquette and Reeder,

1995).

The reaction of calcite with environmental contaminants has been extensively investigated, with many studies focusing on species that are on the U.S. Environmental Protection Agency (U.S.E.P.A.) list of national primary drinking water contaminants. This list comprises inorganic cations and anions and includes heavy metals (cadmium, chromium, copper, lead, mercury and thallium), alkali earth metals (beryllium and barium), non-metals (arsenic and selenium) and anions (cyanide, fluoride, nitrate and nitrite) (Safe Drinking Water Act, 1974). Sorption processes involving calcite with many of these analytes have been reported in the scientific community. The adsorption and transport processes of Cd in calcareous, sandy soils with low organic-matter content were reported to be predominantly controlled by calcite (Martin-Garin et al., 2002). Copper was shown to have a high affinity for the calcite surface, suggesting that calcite could be important in predicting the mobility of Cu in natural systems (Elzinga and Reeder, 2002). Calcite removal of Pb from aqueous solution by sorption processes was shown to occur simultaneously with the release of Ca from the mineral system (Godelitsas et al., 2003). Barium, along with other divalent metal ions, has been reported to be incorporated into the calcite crystal structure during crystal growth by a reaction mechanism that involves adsorption, diffusion and inner-sphere coordination (Reeder, 1996). The substitution of Se as SeO_4^{2-} for CO_3^{2-} in the calcite single crystal structure has been suggested in studies by Staudt et al. (1994).

Arsenic is another extensively studied contaminant on the U.S.E.P.A. list of national primary drinking water contaminants. Arsenic occurs naturally in the environment in many different minerals which are derived from geologic sources such as

igneous and sedimentary rock formations. Arsenic can be introduced into soil, water and air from natural sources in the environment through mineral weathering and volcanic activity. Anthropogenic sources of arsenic contamination to the environment are primarily from timber treatment, waste incineration, coal combustion, metal mining and pesticide applications. Chemical releases of arsenic to the environment can have an adverse effect on the quality of soil, air and water, and the U.S.E.P.A. has recognized arsenic as a priority pollutant and human carcinogen (U.S.E.P.A., 1982). In 2001, the maximum level of arsenic permitted in municipal drinking water was lowered from 50 to 10 $\mu g\ L^{-1}$.

The speciation or chemical structure of arsenic can determine how the compound interacts in the environment and can also determine the toxicity to organisms and humans. Inorganic forms of arsenic [arsenate (iAs^{V}) and arsenite (iAs^{III})] are the most common species in water, soil and sediment and are highly toxic to biological organisms and humans. These inorganic arsenic forms can be biomethylated by microorganisms to form organic arsenicals [monomethylarsonic acid ($MMAs^{V}$), monomethylarsonous acid ($MMAs^{III}$), dimethylarsonic acid ($DMAs^{V}$), dimethylarsonous acid ($DMAs^{III}$), trimethylarsine oxide (TMA^{V}) and trimethylarsine (TMA^{III})] by a mechanism of alternating reduction and oxidative methylation reactions (Figure 1) (Bentley and Chasteen, 2002; Dombrowski et al., 2005; Lafferty and Loeppert, 2005). These biochemical transformations can lead to the occurrence of methylated arsenic in the environment. This process of biomethylation has long been considered to be a detoxification pathway, and the toxicity and transformations of arsenic and methyl arsenic compounds are still being studied and evaluated by the toxicological community

(Vasken, 1997). In addition to the biomethylation of arsenic by microorganisms in the environment, organic arsenicals can be directly applied to the environment from anthropogenic sources such as agricultural pesticides or from poultry and swine waste where arsenic is a trace constituent of the feed additive.

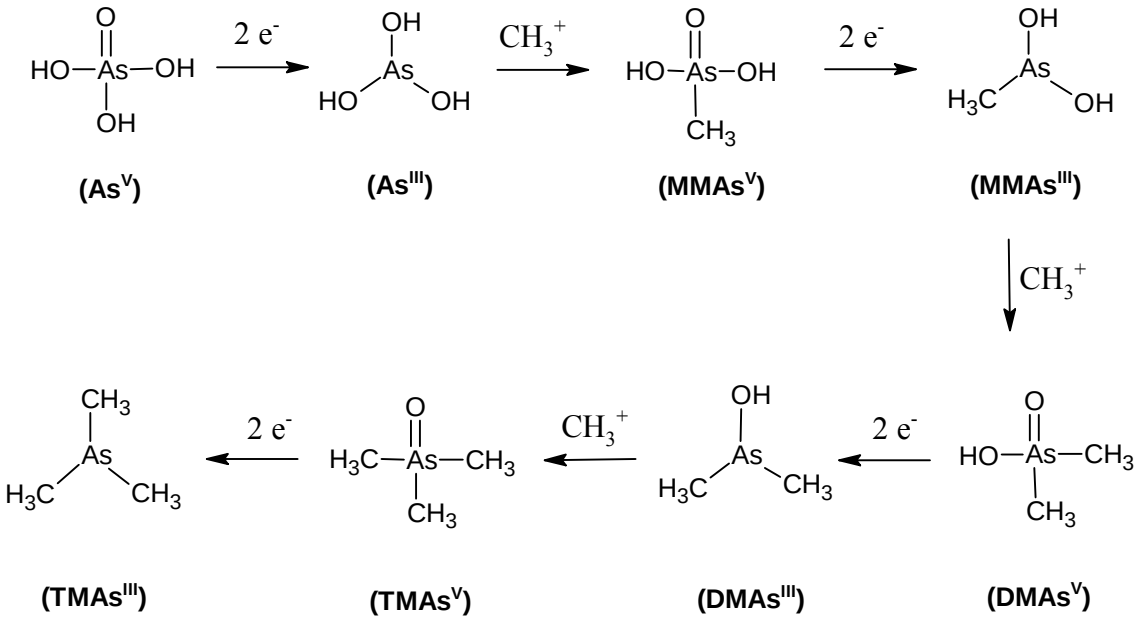

Figure 1. Biomethylation pathway for arsenic showing alternating steps of reduction and oxidative methylation.

The symmetry and charge of dissolved aqueous species of arsenic and methyl arsenic are dependent on the protonation state of the molecule. Protonation states of acids are related to the pH by their respective pK_a values. The pK_a values for iAs^V and iAs^{III} have been reported by Wagman et al. (1982), and the pK_a values for $MMAs^V$ and $DMAs^V$ have been reported by Smith and Martell (1976). These values are listed in Table 3. Each

pKa value represents the pH at which one-half of the given species is dissociated by losing a hydrogen atom from a hydroxyl group to create an oxyanion. (Figure 2).

Table 3. pKa values for arsenic species.

As species	Symbol	pKa_1	pKa_2	pKa_3
$H_3AsO_3^{o}$ †	iAs^{III}	9.22	12.13	13.4
$H_2AsO_3(CH_3)^{o}$ ‡	$MMAs^{V}$	4.19	8.77	§
$HAsO_2(CH_3)_2^{o}$ ‡	$DMAs^{V}$	6.14	§	§
$H_3AsO_4^{o}$ †	iAs^{V}	2.20	6.97	11.53

† (Wagman et al., 1982)
‡ (Smith and Martell, 1976)
§ Unknown or undetermined values

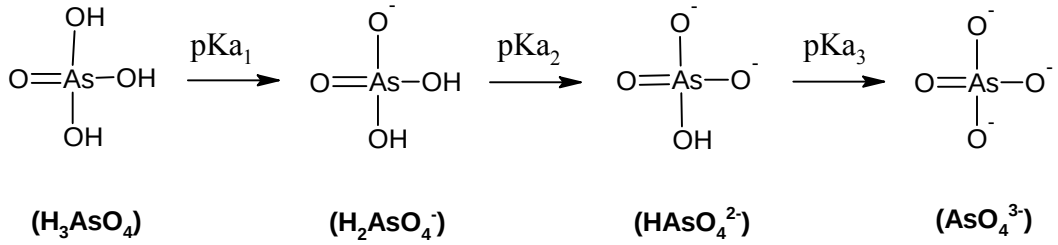

Figure 2. Structural representation showing the steps of deprotonation of inorganic arsenate (iAs^{V}) and the pKa value associated with each step.

The charge of calcite surface sites, ion size and symmetry, and arsenic speciation affect the ability of arsenic to interact at the surface of calcite. Site geometries of calcite functional groups exert a dominant effect on ion incorporation at the calcite surface, especially when considering the geometry and speciation of sorbing molecules (Cheng et

al., 1999). Carbonate functional groups ($>CaCO_3^-$ and $>CO_3^-$) have planar trigonal shape because of delocalized π-bonding, surface water ($>CaOH_2^+$) has a tetrahedral arrangement due to two non-bonding pairs of electrons, and the highly electropositive surface calcium ($>CO_3Ca^{2+}$) has an atomic electronic configuration [Ar] $4s^2$ (Cotton and Wilkinson, 1976). Arsenite (iAs^{III}) has a pyramidal trigonal shape with a non-bonding valence shell electron pair (Cheng et al., 1999). Arsenate (iAs^V) has a tetrahedral arrangement with one non-bonding electron pair and one bonding electron pair (Cotton and Wilkinson, 1976). Methyl substitution for the hydroxyl group in the arsenic anion molecule creates an electron donating effect to the arsenic atom and decreases the polarity and charge density of the molecule. Also, the methyl group can interact by Van der Waals forces (McMurray, 1984).

The mobility of arsenic in a soil environment can be influenced by organic matter and biota, redox conditions, pH, temperature, moisture regime and mineral composition of the soil (Bissen and Frimmel, 2003). The geochemical interaction of arsenic with mineral surfaces has been extensively studied, and sorption to calcite and other minerals, especially iron oxides, has been suggested as the likely controlling factor of these compounds in soil and groundwater environments (Romero et al., 2004). The adsorption of arsenic in a calcareous, montmorillonitic soil was shown to be significantly reduced by the removal of carbonates, suggesting that calcite plays a major role in the adsorption of arsenic (Goldberg and Glaubig, 1988). Le Guern et al. (2003) found arsenic to be sequestered and trapped during coprecipitation with carbonates in hydrothermal spring waters.

The arsenate analog, phosphate, is similar in its chemical properties, and both are

listed in the nonmetals group 5A of the periodic table. Phosphate adsorption to calcite was studied by Celi et al. (2000), and it was suggested that sorption occurs by chemisorption at low concentrations of phosphate and by surface precipitation at high concentrations of phosphate. Millero et al. (2001) suggested that phosphate sorption occurs by chemisorption followed by a slow transformation to an amorphous surface phase, with subsequent precipitation of a crystalline secondary phase.

Arsenic adsorption by calcite has also been studied for use in water and waste treatment applications. Song et al. (2006) demonstrated the utility of calcite as a secondary particle in the coagulation of ferric hydroxide and arsenic. Ohki et al. (1996) showed that limestone could be loaded with Al^{3+} and Fe^{3+} to adsorb inorganic and organic forms of arsenic from solution. In the waste treatment study by Dutre and Vandecasteele (1998), an increase in the amount of lime added to metallurgical, ash-cemented wastes was shown to decrease the ability of arsenic to be leached from the waste, probably due to the formation of calcium arsenate. Bothe and Brown (1999a) studied the X-ray diffraction patterns of solid phase calcium arsenates that formed from the reaction of arsenic with lime, and the following solid phases formed in order of decreasing pH: $Ca_4(OH)_2(AsO_4)_2 \cdot 4\ H_2O$, $Ca_5(AsO_4)_3OH$ (arsenate-hydroxy-apatite), $Ca_3(AsO_4)_2 \cdot 3\ ^2/_3\ H_2O$, $Ca_3(AsO_4)_2 \cdot 4\ ^1/_4\ H_2O$, $Ca_5H_2(AsO_4)_4 \cdot 9\ H_2O$ (ferrarisite), $Ca_5H_2(AsO_4)_4 \cdot 9\ H_2O$ (guerinite) and $CaHAsO_4 \cdot H_2O$.

Empirical isotherm models are commonly used to describe the sorption processes that occur between a sorbing mineral and a solute species of interest. Isotherm models such as the Freundlich or Langmuir isotherms have a wide range of application and can be used to give a quantitative, mathematical description of the mass distribution of a

substance between the solid and solution phases at equilibrium. Adsorption isotherms alone cannot indicate whether adsorption or precipitation is the mechanism of reaction, and further spectroscopic investigation is usually required to deduce such information (Veith and Sposito, 1977). The Freundlich equation (Freundlich, 1926) was initially developed to describe the precipitation of colloid suspensions by electrolytes and is empirical in nature without a theoretical foundation. The general form of the equation is represented by equation [2], in which q represents the amount of species adsorbed per amount of adsorbate, C_{eq} is the concentration of adsorbate at equilibrium in solution, and K_f and n are constants.

$$q = K_f(C_{eq})^n \qquad [2]$$

The linear form of equation [2] can be obtained by performing a logarithmic transformation and yields equation [3] with a y-intercept of log K_f and a slope of n.

$$\log q = \log K_f + n \log C_{eq} \qquad [3]$$

By using this form of the Freundlich equation, a linear regression analysis of the adsorption data, where q and C_{eq} are measured and known, can be used to determine the constants K_f and n. A prediction equation can then be generated to describe the adsorption behavior, and the predictability of this equation in describing the adsorption data can be represented by the coefficient of determination, R^2, which indicates the strength of the linear relationship between C_{eq} and q (Ott and Longnecker, 2001).

The Langmuir equation (Langmuir, 1918) presented as case I in the original paper is also known as the "Langmuir Isotherm" and was theoretically derived to describe the monolayer adsorption of gas molecules on a solid surface, whereby an adsorption maximum is achieved as the monolayer is filled. The general form of the equation is represented by equation [4], in which q represents the amount of species adsorbed per amount of adsorbate, C_{eq} is the equilibrium concentration of adsorbent in solution, b is the adsorption maximum and K_L is the adsorption constant (Essington, 2003).

$$q = (bK_LC_{eq}) / (1 + K_LC_{eq}) \quad [4]$$

The linear form of equation [4] can be obtained by performing a logarithmic transformation and yields equation [5] with a y-intercept of $1/bK_L$ and a slope of 1/b.

$$C_{eq} / q = (1 / bK_L) + (C_{eq} / b) \quad [5]$$

By using this form of the Langmuir equation, a linear regression analysis of the adsorption data where q and C_{eq} are measured and known can be used to determine the adsorption maximum, b and the adsorption constant K_L.

Chemical equilibrium models are typically employed to study the speciation of aqueous phase ions and can be used to study the saturation state with respect to hypothetical or actual solid-phase components in multi-component equilibrium systems. The first chemical equilibrium model used to study ion speciation in natural waters was developed by Garrels and Thompson (1962). Since its inception, many models have been

developed to evaluate the concentration and speciation of contaminants in groundwater and surface water media. MINTEQA2 (Allison et al., 1991) is a geochemical assessment model that was developed by the U.S.E.P.A. and can be used to predict the equilibrium distribution of dissolved aqueous, adsorbed and solid phase species in the laboratory or in natural aqueous systems. MINTEQA2 uses an extensive thermodynamic database and the known total concentrations of components in the system to make an initial estimate of the activity of each component in the system. MINTEQA2 then calculates the concentration of each species using the mass law equation [4], in which C_i is the concentration of species *i*, K_i is the equilibrium constant of species *i*, γ_i is the activity coefficient of species *i*, X_j is the activity of component *j*, $a_{i,j}$ is the stoichiometry of component *j* in species *i*, and *n* represents the number of components in the species.

$$C_i = (K_i / \gamma_i) \prod_{j=1}^{n} X_j^{ai,j} \qquad [4]$$

MINTEQA2 then calculates the total mass for each component from the concentrations of every species containing that component using mass balance equation [5] in which Y_j is the mass imbalance and T_j is the known total concentration of each component.

$$Y_j = \sum_{i=1}^{m} a_{i,j} C_i - T_j \qquad [5]$$

The calculated total mass is then compared to the known total mass, and if the difference is more than an established tolerance limit then a new estimate of the activity of each component is used until mass imbalance meets the acceptance criterion. Once the computational, iterative process has been completed, MINTEQA2 generates an output that presents the saturation state with respect to hypothetical solid phases, which can be used to estimate solid phases likely to control solubility of the species of interest. MINTEQA2 can also perform sensitivity analyses with respect to various environmental parameters. In addition to characterizing the speciation of contaminants in a multi-phase, multi-component, equilibrium system, MINTEQA2 also has the ability to calculate the distribution coefficient, K_d, between adsorbed and dissolved concentrations which is useful in contaminant transport modeling and risk assessment of contaminants in groundwater and surface water environments.

OBJECTIVES

The primary focus of this research is to investigate the interaction of arsenic with calcite. The carbonate sample will initially be characterized to verify mineralogy and to enable an evaluation of the influence of particle size on arsenic adsorption. Adsorption kinetics for the adsorption of arsenate (iAs^{V}) to calcite will be examined in order to determine reaction rate characteristics such as temporal changes in rate and variability versus iAs^{V} concentration. The retention of various species of arsenic: arsenate (iAs^{V}), arsenite (iAs^{III}), monomethylarsonic acid ($MMAs^{V}$) and dimethylarsonic arsenic acid ($DMAs^{V}$) will be evaluated for adsorption to calcite using adsorption isotherms. The impact of some common groundwater species such as dissolved calcium (Ca^{2+}), magnesium (Mg^{2+}), phosphate and sulfate on arsenic adsorption will be assessed using adsorption isotherms, and the comparative adsorption of phosphate and arsenate will be evaluated. Adsorption isotherms will be used to mathematically describe and quantify the adsorption reactions. Aqueous speciation and solubility relations of arsenate upon reaction with calcite and the possible formation of calcium arsenates will be evaluated using MINTEQA2 by imputing data for batch pH, alkalinity, and dissolved calcium and arsenic concentrations. Implications of these reactions to calcite sorption behavior in soil and groundwater environments will be discussed.

MATERIALS AND METHODS

Chemicals

Research grade calcite from a natural calcite deposit in Santa Eulalia, Chihuahua, Mexico was obtained from Ward's Natural Science Establishment (Rochester, NY). Reagent grade calcite lot A and lot B were obtained from Alfa Aesar (Ward Hill, MA). Reagent grade inorganic arsenic compounds (iAs^{V} and iAs^{III}) were obtained as oxides (As_2O_5 and As_2O_3) from Alfa Aesar (Ward Hill, MA). Monomethylarsonic acid ($MMAs^{V}$) was obtained as a sodium salt (monosodium acid methane-arsonate sesquihydrate, $CH_4AsNaO_3 \cdot 1^1/_2\ H_2O$) and dimethylarsonic acid ($DMAs^{V}$) was obtained in acid form (dimethylarsonic acid, $C_2H_7AsO_2$), both from Chem Service (West Chester, PA). Calcium nitrate, 4-hydrate crystal ($Ca(NO_3)_2 \cdot 4\ H_2O$) was obtained from Mallinckrodt Baker (Phillipsburg, NJ). Reagent grade magnesium nitrate, 6-hydrate crystal ($Mg(NO_3)_2 \cdot 6\ H_2O$) and sodium sulfate (Na_2SO_4) were obtained from Fisher Scientific (Fair Lawn, NJ). Reagent grade sodium phosphate dibasic (Na_2HPO_4) was obtained from EM Science (Gibbstown, NJ).

Particle Size Analysis

Particle-size analysis was performed using the Beckman Coulter (Fullerton, CA), LS 13 320, laser-diffraction particle-size analyzer with a 750 nm laser beam. The instrument measures the particle-size distribution from 0.045 – 2000 μm. The laser beam accurately measures particles > 0.4 μm but uses the polarization intensity differential of scattered light to measure particle sizes from 0.045 – 0.40 μm. The natural calcite was ground using a mortar and pestle before analysis. Dry calcite samples were weighed and

then prepared as suspensions in 10 mL of deionized water before introduction into the instrument. The calcite suspension was mixed thoroughly and quickly added to the sample chamber to assure a representative composition. Sample was added until the required light intensity was achieved for sample analysis. Dispersion of the calcite particles was achieved by ultrasonication for 10 min at the highest energy setting within the aqueous liquid module before the particles were introduced into the sample chamber for analysis. The Mie theory optical model (Eshel et al., 2004) with a calcite refractive index of 1.6583 was used to calculate particle-size distribution, and the results were reported as a percent of the total volume of solid.

Electron Microscopy

Electron microscopy was performed using the JEOL (Tokyo, Japan), JSM-6400, scanning electron microscope. Samples were prepared by fixing dry calcite to an aluminum sample stub by using conductive tape. The sample was then coated with gold to reduce charge buildup on the sample particles. Digital images were captured using the secondary electron imaging mode. The images were generated using a digital resolution of 2056 dpi. The image magnification ranged from 2300 to 15000x with a spatial resolution of 3.5 nm.

X-ray Diffraction

X-ray diffraction was performed using the Philips Electronic Instruments (Mahwah, NJ) Norelco model 12215/0 X-ray diffractometer with CuKα radiation operated at 35 kV and 40 mA. Power was supplied to the Norelco generator by a Norelco

dual HV power supply set at 1706 V. Samples were prepared by grinding the calcite with a mortar and pestle and placed into the x-ray slide such that a random orientation of crystals was achieved. The slide was placed into the mount for analysis, the goniometer was set at 2 degrees 2-theta, and the x-ray scan was performed to 65 degrees 2-theta. The signal was processed using the Phillips Electronic Instruments data processor, and the data files were converted to Microsoft (Redmond, WA) Excel and graphed as counts per second versus degrees 2-theta.

Adsorption Kinetics

The adsorption kinetics experiments were performed using synthetic calcite lot A in duplicate reactions. Batch reaction vessels were 100 mL, high-density, polyethylene containers with screw-top caps. A small hole was drilled into the caps to allow for equilibration with ambient air and to ensure minimum loss of aqueous volume by evaporation. One ($\pm$ 0.0010) gram of calcite was weighed and added to 50.0 ($\pm$ 0.1) mL of MilliQ deionized water (> 16 megaohm-cm). The reaction vessels were placed in a reaction chamber on a mechanical shaker at 200 oscillations per minute and kept at a constant reaction temperature of ~ 25^{o}C. All suspensions were allowed to equilibrate for at least 48 h before the addition of arsenic. As^{V} stock solution was prepared at a concentration of 0.044 M and adjusted to a pH of 8.2. As^{V} spiking solutions were prepared as dilutions from the stock solution and adjusted to a pH of 8.2. The initial kinetics experiment was performed at seven different As concentrations in the calcite suspension: 0.09 μM, 0.18 μM, 0.44 μM, 0.87 μM, 1.8 μM, 4.4 μM and 8.7 μM. Aliquots of 500 μL for the initial, kinetics evaluation were taken at 1, 8, 24, 48, 120

hours of reaction and diluted to a final volume of 1500 µL. The second kinetics experiment was performed at both a low initial arsenic concentration of 4.4 µM and a high initial arsenic concentration of 263 µM. Aliquots of 200 µL for the second kinetics experiment were taken at 0.017, 0.033, 0.083, 0.167, 0.333, 0.5, 0.667, 0.833, 1, 2, 3, 4, 6, 8, 24, 48, 72 and 96 hours of reaction and diluted to a final volume of 1200 µL. All samples were diluted and analyzed by inductively coupled plasma mass spectrometry (ICP-MS). Adsorbed arsenic was calculated as the difference between the quantity of initial arsenic in solution and the equilibrium quantity of arsenic. Adsorption kinetics was plotted as mass or percent arsenic adsorbed versus time.

Adsorption Isotherms

All adsorption isotherms were performed as batch experiments using synthetic calcite lot A. Adsorption isotherm reactions were performed in duplicate. The experimental setup was the same as with the kinetics studies. All suspensions used in the adsorption studies were allowed to equilibrate for at least 48 h before the addition of other reagents. Calcium and magnesium solutions (0.1 M or 0.01 M initial concentration as the nitrate salts) were added and allowed to equilibrate for 24 h before the addition of arsenic in the studies of the effects of these respective ions. Phosphate and sulfate solutions were added simultaneously as molar equivalents with arsenic in the competitive adsorption studies. As^{V} stock solution was prepared at a concentration of 0.044 M, As^{III} stock solution was prepared at 0.038 M, MMA^{V} stock solution was prepared at 0.045 M, and DMA^{V} stock solution was prepared at 0.045 M. All stock solutions were adjusted to a pH of 8.2. Arsenic spiking solutions were prepared as dilutions from the stock solution

and adjusted to a pH of 8.2. Initial concentrations ranged from about 0.1 μmol to 13.5 μmol in the calcite suspensions. The corresponding range of molar ratios was about 5.0 x 10^{-07} to 6.75 x 10^{-05} moles of arsenic per mole of calcite. The calcite suspensions were allowed to react with arsenic for 24 h before aliquots of the mixture were taken for analysis. Samples were diluted and analyzed by ICP-MS. Adsorbed arsenic was calculated from the difference between the concentration of initial arsenic and the final concentration of equilibrium dissolved arsenic. Adsorption isotherms were plotted as mass or percent arsenic adsorbed versus initial or equilibrium arsenic concentration.

Modeling of Adsorption Isotherms

Linear regression analysis of the adsorption isotherm data was performed using the linear form of the Freundlich equation (equation [3]). SPSS (Chicago, IL) statistical software was used to calculate the regression coefficients (n and log K_f) by using log q as the dependent variable and log C_{eq} as the independent variable. The calculated constants n and K_f were then used in the Freundlich equation [2] to plot the model versus the experimental data. Linear regression analyses were also conducted on adsorption isotherm data by using the linear form of the Langmuir equation [5]. The regression coefficients (b and K_L) were calculated by using C_{eq}/q as the dependent variable and C_{eq} as the independent variable. The calculated adsorption maximum b and adsorption constant K_L was then used in the Langmuir equation [4] to plot the model versus the experimental data. The fit of the linear forms of the Freundlich and Langmuir adsorption models are represented by the coefficient of determination, R^2.

Arsenic Analysis

Arsenic analysis was performed using a Perkin Elmer (Wellesley, MA) ELAN DRC II inductively coupled plasma mass spectrometer (ICP-MS). A daily performance evaluation of the instrument operation was conducted prior to each analysis by analyzing a 1 ppb standard of yttrium, cerium and barium. The performance criteria for acceptance of instrument operation were an yttrium count of 20,000 or greater, cerium oxide percent less than 4.0 percent of cerium intensity and doubly-charged barium percent less than 3.0 percent of barium intensity. The mass spectrometer was operated in analog mode to give a linear range of over 5000 ppb. Aliquots were taken from the reaction vessels and diluted to an appropriate volume consistent with the linear range and calibration. Calibration was performed using a reagent blank and a 5 point calibration curve. Yttrium was used as the internal standard, and all results were corrected based on the internal standard recovery. Method blanks were analyzed for each experimental batch, and continuing calibration verification (using acceptance criteria of $\pm$ 10%) was performed before and after each batch on the midpoint calibration standard.

Calcium Analysis

Calcium analysis was performed using a Perkin Elmer (Wellesley, MA) AAnalyst 400 flame atomic absorption spectrometer. The instrument was operated using air-acetylene with gas flow rates of 10 L/min for air and 2.7 L/min for acetylene. A calcium hollow cathode lamp was used and operated at 6 mA. A wavelength of 422.7 nm and a spectral slit width of 0.7 mm were utilized for analysis. The software for analysis was WinLab32 for AA, version 6.0.0.0065. For calibration curves, standards of 2, 5, 10 and

20 mg Ca L^{-1} were used. All samples and standards were treated with 1000 mg L^{-1} KCl ionization suppressant. The method sensitivity was 2 μg L^{-1}, and a standard of 5 mg L^{-1} was used for continuing calibration verification with a quality control acceptance criterion of 90 – 110 % recovery.

Alkalinity Determination

Alkalinity determination was performed using a Radiometer Copenhagen (Copenhagen, Denmark) TIM 900 titration manager with a pHG201 glass combination electrode. The instrument was calibrated using VWR Scientific (West Chester, Pennsylvania) pH buffer solutions of pH 4.00 and 7.00 which bracketed the sample pH. Acceptable calibration criteria required buffer readings to be within 0.05 pH units of each buffer's true value. Sample aliquots of 12 mL were titrated manually to the bicarbonate endpoint of pH 4.5 with 0.02 M HCL using a 100 μL Eppendorf micropipette. Continuing calibration verification was performed after each 10 sample analyses with an acceptance criteria of $\pm$ 0.1 pH unit for each buffer solution.

Chemical Equilibrium

Chemical equilibrium was evaluated using chemical equilibrium and speciation program MINTEQA2 (Allison Geoscience Consultants, Flowery Branch, GA), version 1.50 for windows. The input parameters used for the equilibrium model included pH, alkalinity, temperature and species concentrations. The pH was measured and entered as equilibrium pH, alkalinity was measured at equilibrium and entered as meq L^{-1}, temperature was measured and entered as degrees Celsius, and calcium and arsenic were

measured at equilibrium and entered as molar concentrations. Activity coefficients were calculated using the Davies equation and species activities were used for the equilibrium model calculations. The thermodynamic database was edited to include log K values for some dissolved, aqueous species and the pK_{sp} values of relevant calcium arsenate, solid phases as presented by Bothe and Brown (1999). MINTEQA2 was used to calculate concentration and activity of all dissolved, aqueous species and the saturation states with respect to calcite and all possible arsenate and phosphate containing solid phases.

RESULTS AND DISCUSSION

Calcite Characterization

Two different lots of synthetic calcite were analyzed for particle-size distribution by laser diffraction and by scanning electron microscopy. The certificate of analysis from the manufacturer listed calcite lot A as 99.99% calcium carbonate on a metals basis and calcite lot B as 99.95% on a metals basis, with the trace elemental analysis for each lot listed in Table 4.

Table 4. Trace element content of calcite lot A and calcite lot B.

Analyte	Calcite Lot A†	Calcite Lot B†	Analyte	Calcite Lot A†	Calcite Lot B†
Assay (metals basis)	99.99%	99.95%	Iron	5 ppm	5 ppm
Barium	15 ppm	2 ppm	Chlorine	‡	42 ppm
Magnesium	8 ppm	7 ppm	Sulfur	‡	12 ppm
Sodium	10 ppm	32 ppm	Arsenic	‡	‡
Strontium	13 ppm	58 ppm	Phosphorus	‡	‡

† Data from Alfa Aesar (Ward Hill, MA) certificates of analysis
‡ Not detected

Calcite lot B had higher sodium, strontium, chloride and sulfur concentrations than those of lot A. The particle-size distributions for calcite lot A and B as determined by laser diffraction are shown in Figure 3 and Figure 4, respectively. The mean particle diameter of calcite lot A was 6 µm, with 2.9 % of the particles by volume in the range from 0.4 – 0.6 µm, 92.8% of the particles in the range from 1.8 – 11.8 µm, and 4.2% of the particles in the range from 14.3 – 22.7 µm. The SEM images of calcite lots A

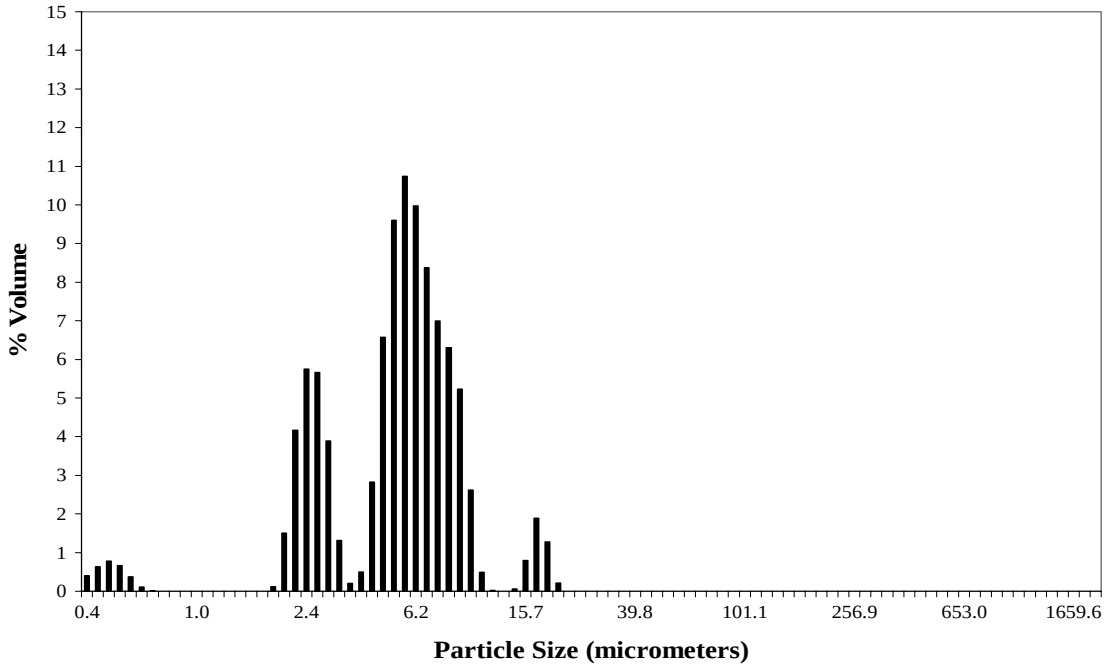

Figure 3. Particle size distribution of calcite lot A as determined by laser diffraction. The mean particle diameter is 6 µm.

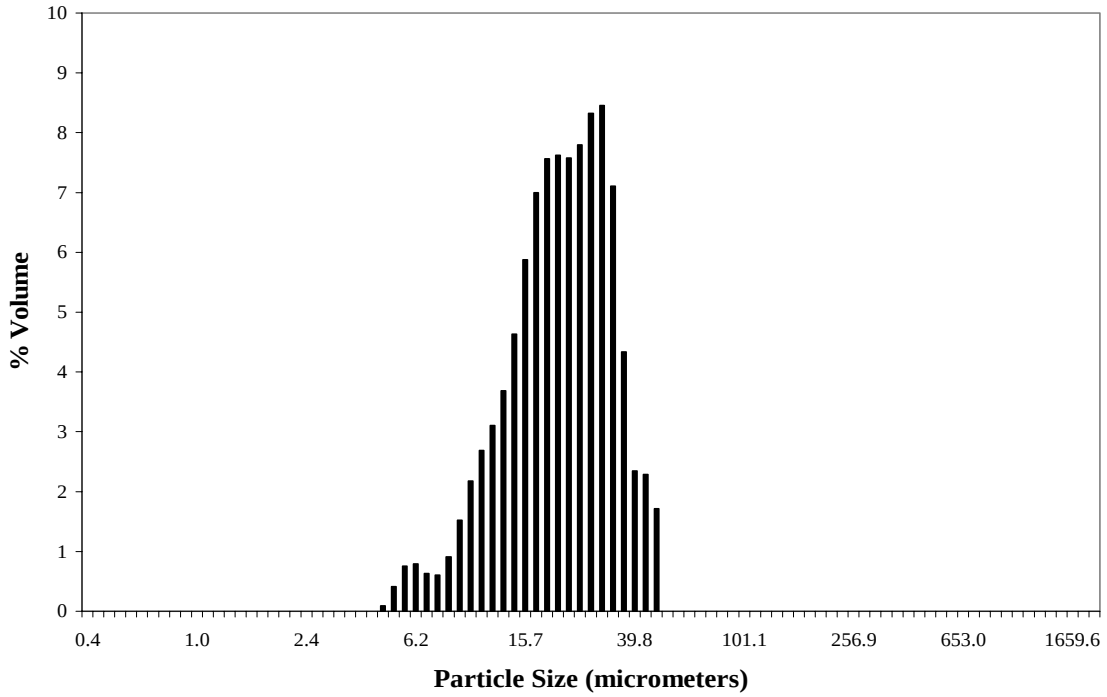

Figure 4. Particle size distribution of calcite lot B as determined by laser diffraction. The mean particle diameter is 24 µm.

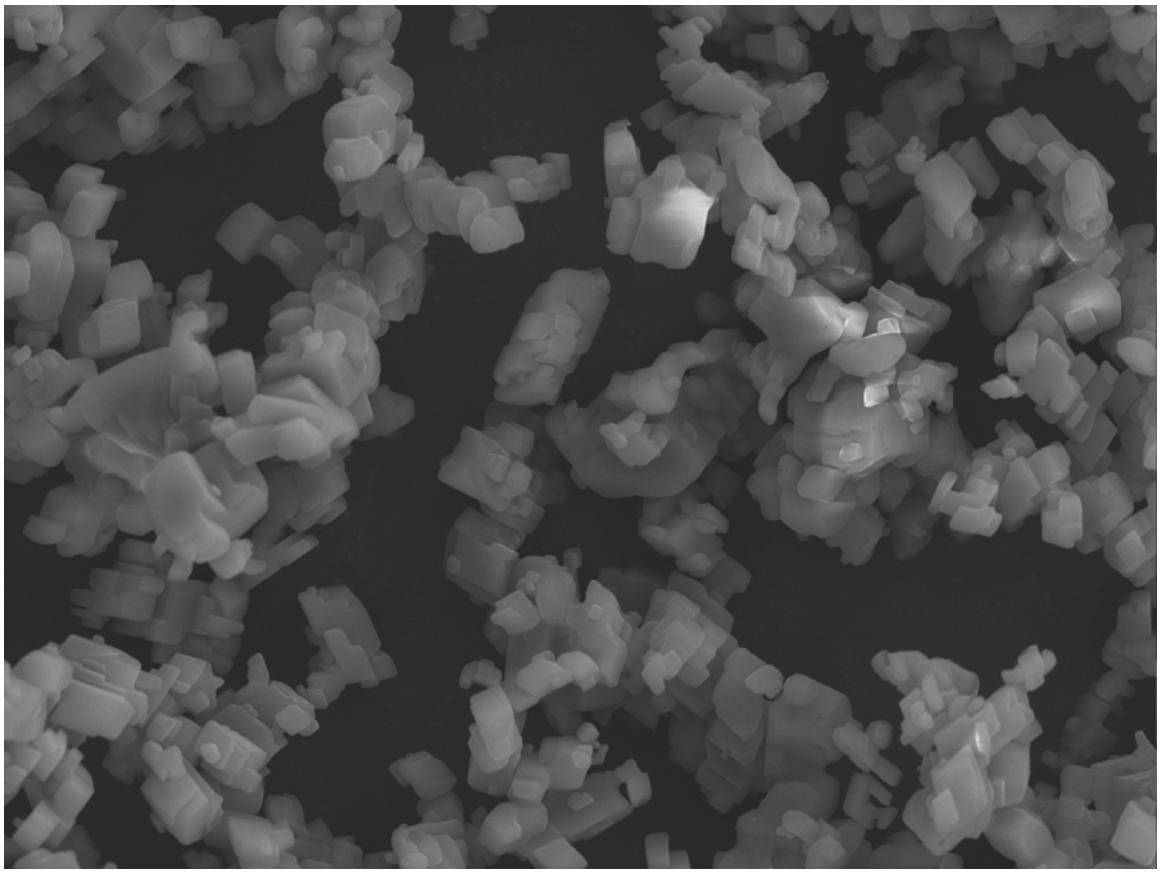

Figure 5. Scanning electron microscopy image of calcite lot A at 3000x magnification. The particle size scale bar line is shown at the bottom left of the image.

(Figure 5) and B (Figure 6) indicate that the individual calcite particles are considerably smaller than 10 µm particle diameter. and qualitatively confirms the laser diffraction particle-size distribution results shown in Figure 3. The SEM images indicate that the particle-size for calcite lot B is smaller than that for calcite lot A, though the aggregate size is larger.

The calcite samples in the images were prepared by fixing dry calcite to an aluminum sample stub, and then the samples were coated with gold to reduce charge

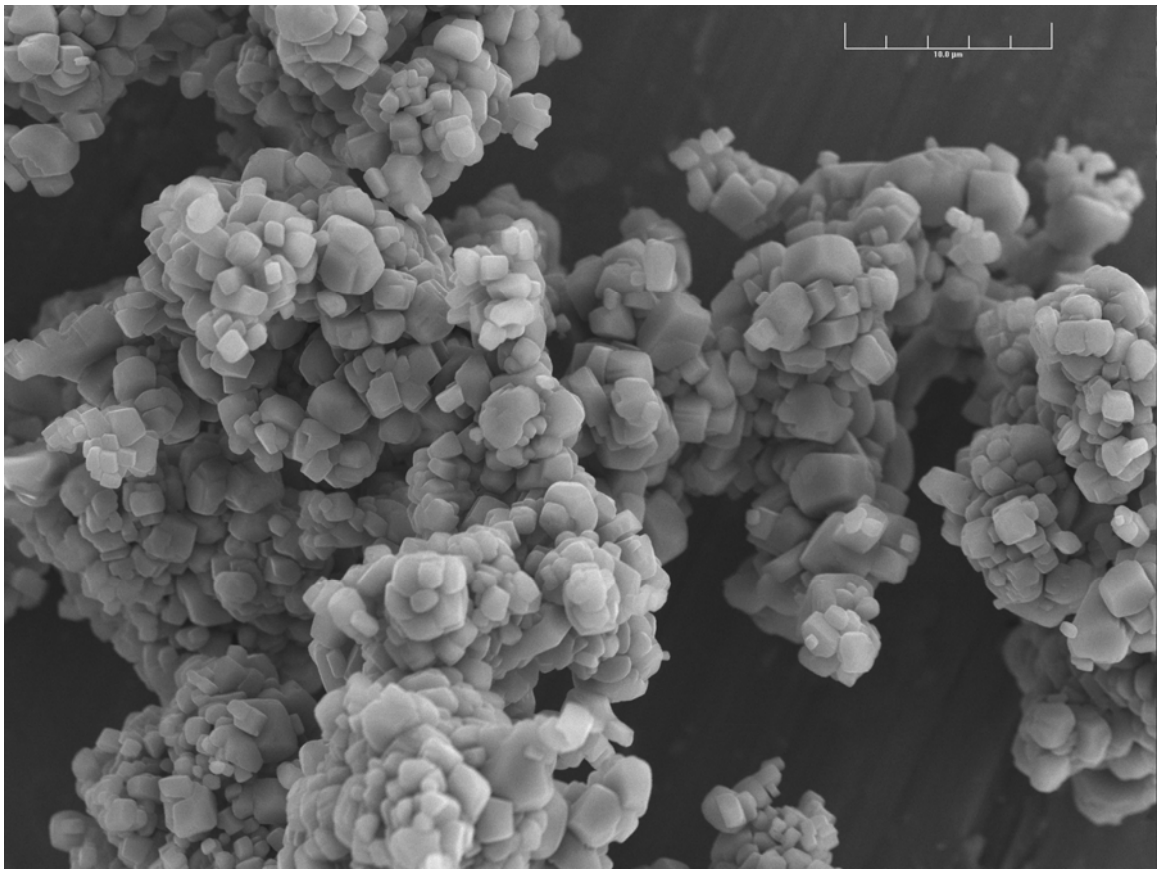

10 µm

Figure 6. Scanning electron microscopy image of calcite lot B at 2300x magnification.

buildup on the sample particles. The particles in the SEM image for calcite lot B appear to be more highly aggregated that those in calcite lot A. The surface structure for calcite in air, when the relative humidity is greater than 60%, is identical to the surface structure of calcite in water and consists of hydroxyl groups and water that can hydrogen-bond to other calcite particles to result in interparticle bonding and aggregation (Fenter et al., 1999). The SEM images of calcite in air show that calcite lot B has a higher degree of interparticle bonding and aggregation than calcite lot A under the same atmospheric conditions. The laser particle-size distribution of calcite lot B is much greater than the

particle size results from the SEM image. This comparison substantiates that the particles in calcite lot B have a higher degree of aggregation than those in lot A. The ultrasonic treatment for 10 minutes at the highest energy setting was not sufficient to disperse aggregates in lot B. The enhanced interparticle bonding and aggregation of calcite lot B could have been impacted by its higher anion content, sulfate and chloride, as summarized in Table 4.

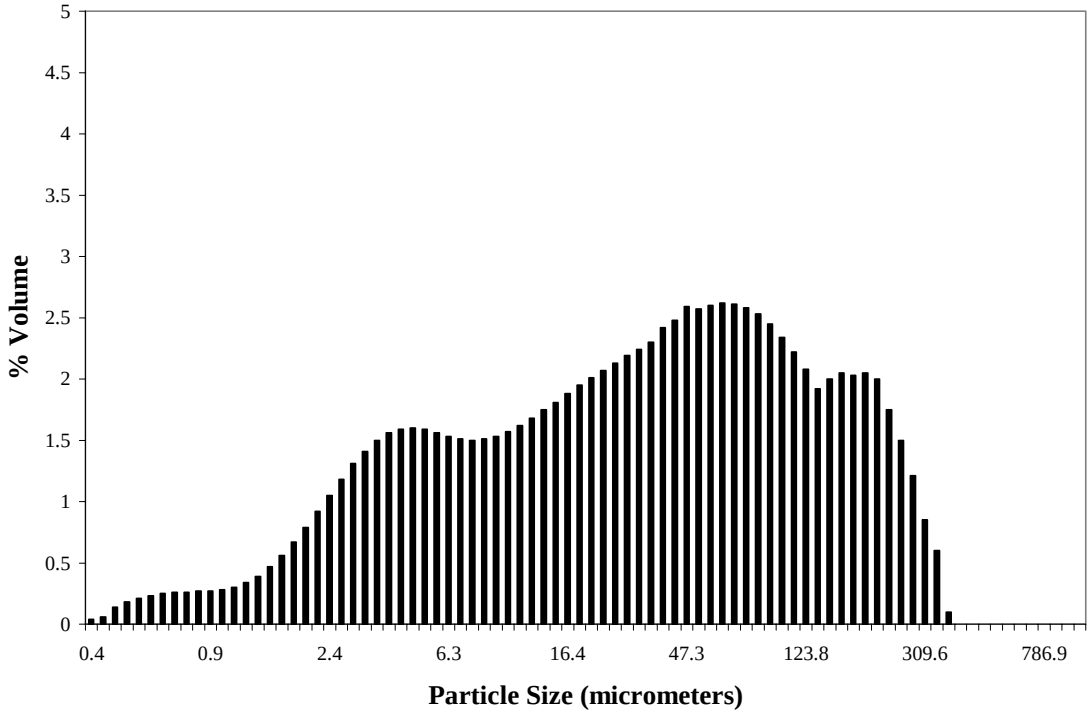

Figure 7. Particle size distribution of ground, natural calcite. The mean particle diameter is 30 µm.

The particle-size distribution for ground, natural calcite is shown in Figure 7 and has a mean particle diameter of approximately 30 µm. The size distribution for the synthetic calcite had a much narrower range about the mean whereas the size distribution

for the natural calcite had a wide range about the mean yielding some particles with a relatively large particle size up to 370 µm.

The synthetic calcite lot A and ground, natural calcite were analyzed by X-ray diffraction, and the patterns are shown in Figure 8. The X-ray diffraction patterns confirm

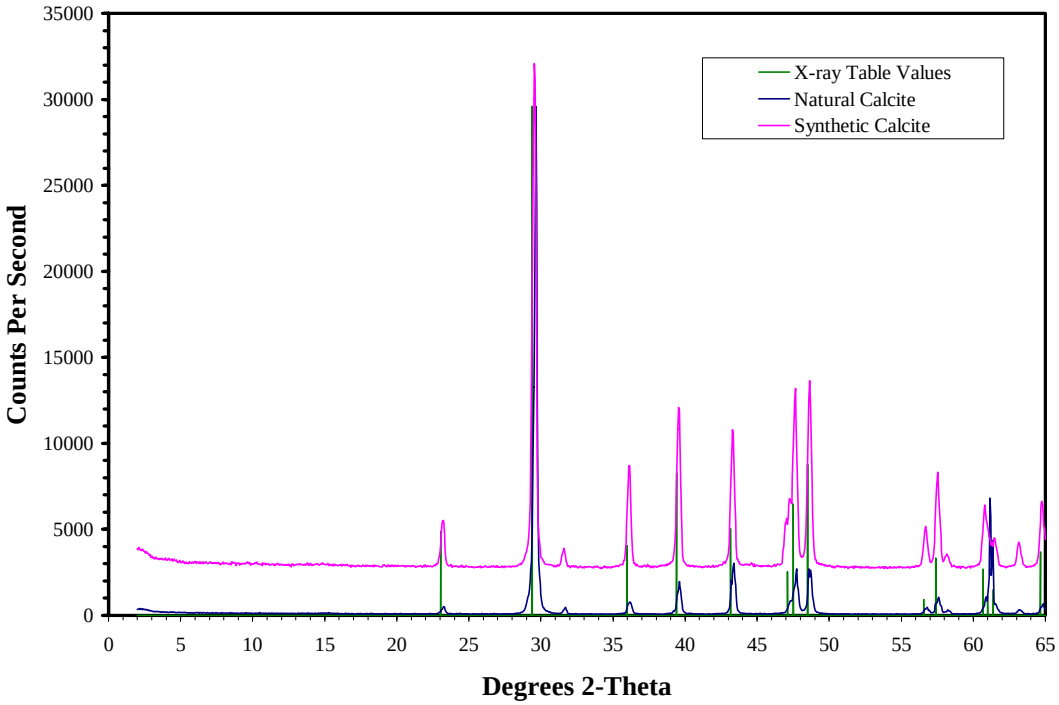

Figure 8. X-ray diffraction pattern for synthetic calcite lot A and ground, natural calcite.

the identification of each calcite sample by its comparison to the calcite peaks listed in the JCPDS – International Centre for Diffraction Data (Newtown Square, PA) X-ray powder data files. The data file table listing for calcite d-spacings represented as degrees 2-theta are shown as sticks in the figure. The three, primary, d-spacing values (degrees 2-theta) for confirmation are at 3.035 (29.45^{o}), 2.095 (43.2^{o}) and 2.285 (39.45^{o}).

Adsorption of iAs^V by Calcite

Twenty-four hour iAs^V adsorption isotherms were performed with both calcite lot A and ground, natural calcite. For the adsorption isotherms plotted as equilibrium dissolved arsenic concentration versus the mass of arsenic adsorbed, iAs^V was adsorbed in a greater amount on synthetic calcite (lot A) than on natural calcite at all equilibrium dissolved arsenic concentrations (Figure 9). When the adsorption isotherm was plotted as

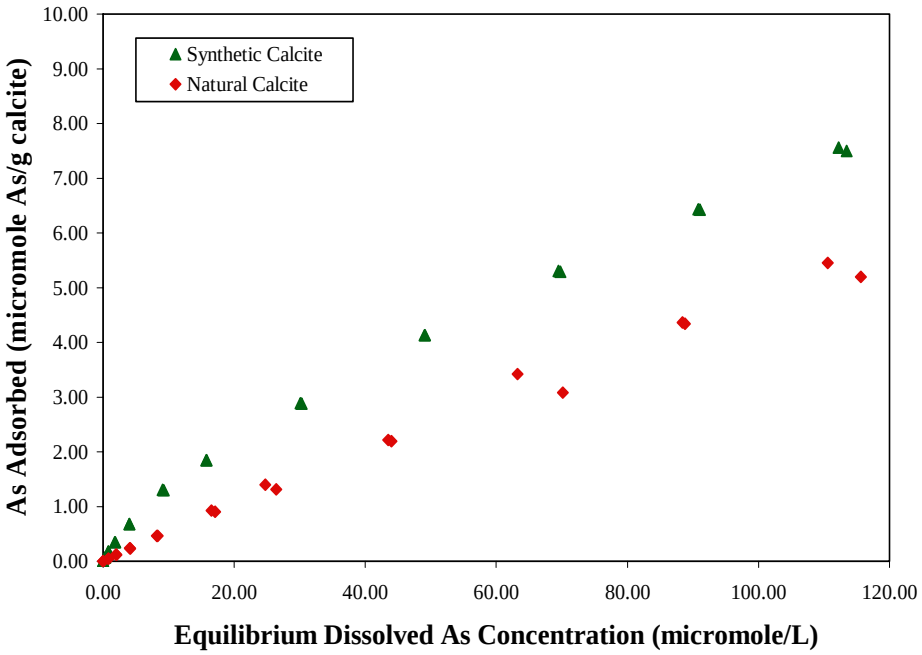

Figure 9. Adsorption isotherms for synthetic calcite (lot A) and natural calcite plotted as the mass of arsenic, iAs^V, adsorbed versus equilibrium dissolved arsenic concentration.

the percent of arsenic adsorbed versus the initial concentration of arsenic, the adsorption of iAs^V was greater than 80% on synthetic calcite as compared to 54 - 55% for natural calcite at < 10 µM initial arsenic concentrations (Figure 10). As the initial concentration

of iAs^V was increased to more than 250 µM, the percent of iAs^V sorbed to the synthetic and natural calcite converged to within 8.0% of each other.

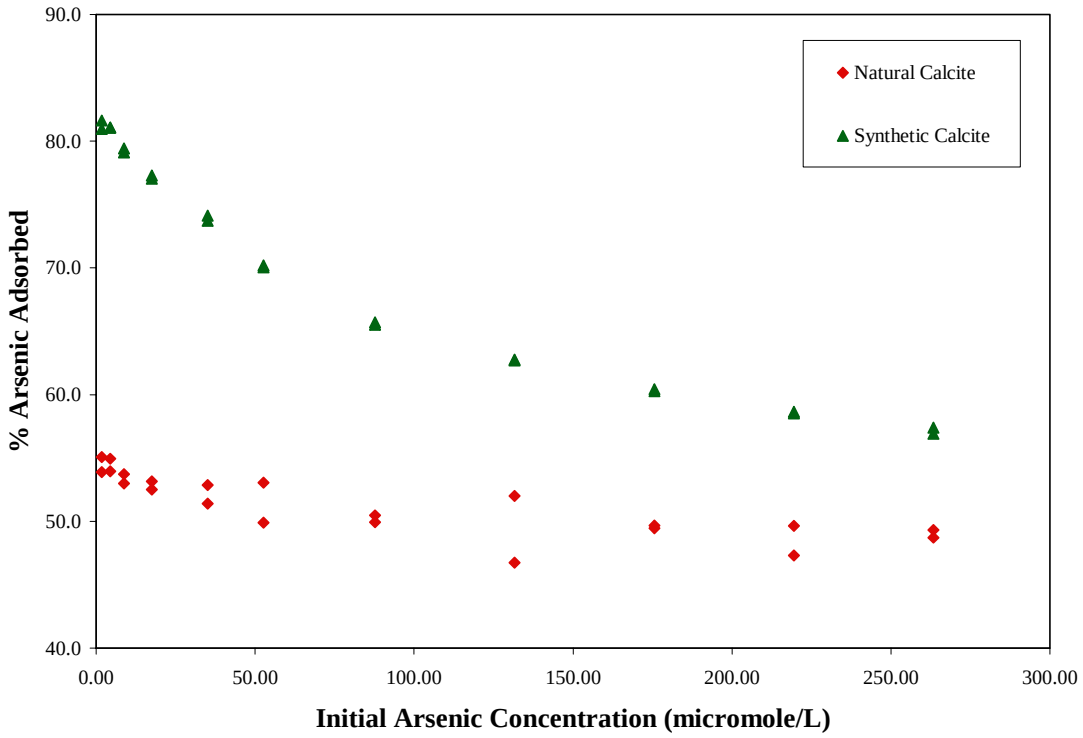

Figure 10. Adsorption isotherms for synthetic calcite (lot A) and natural calcite plotted as the percent of arsenic, iAs^V, adsorbed versus initial arsenic concentration.

The results of the particle-size distribution for the two types of calcite confirmed the hypothesis that a larger particle size, which gives a smaller surface area for adsorption and interaction with iAs^V, would adsorb less arsenic. This effect was pronounced at low equilibrium concentrations of iAs^V, where direct surface interaction is thought to play a critical role, but was less pronounced at higher dissolved iAs^V concentrations. These results indicate that calcite surface area might have played a less important role in iAs^V retention at high dissolved As concentration, possibly due to an increased role of calcium

arsenate precipitation.

Adsorption Kinetics

Kinetics Experiment #1. An initial kinetics experiment was performed in order to

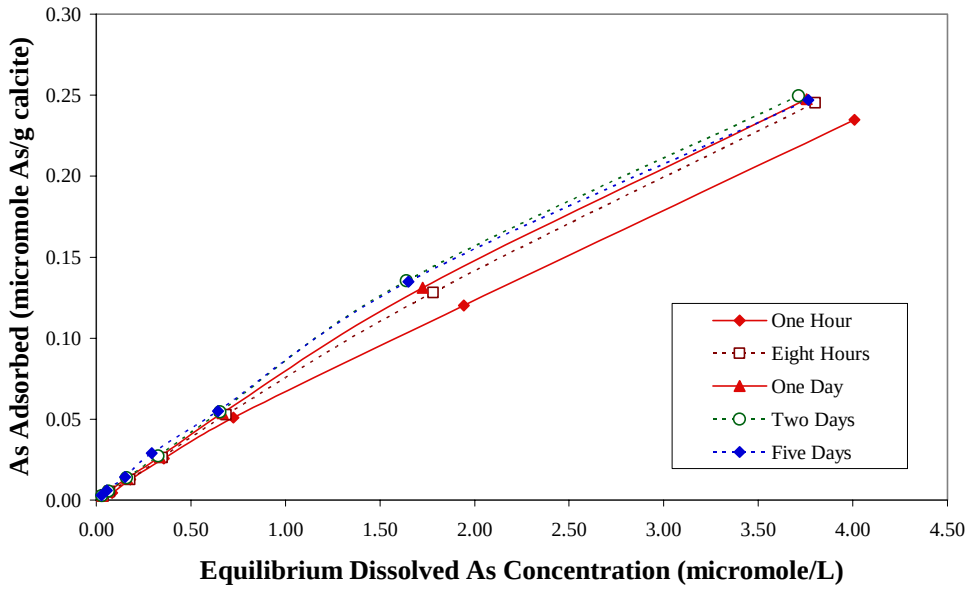

Figure 11. Adsorption kinetics for iAs^V plotted as the mass of arsenic adsorbed versus equilibrium dissolved arsenic concentration.

evaluate the change in iAs^V adsorption as a function of concentration and time. The experiment was designed to evaluate the adsorption of seven different iAs^V concentrations (spanning 2 orders of magnitude) at 1 hour, 8 hours, 24 hours, 48 hours and 120 hours. The results are shown in Figure 11 and expressed as the amount of iAs^V adsorbed versus the equilibrium dissolved iAs^V concentration. The amount of iAs^V adsorbed at one hour was substantially less than the amounts adsorbed at 8 hours or more.

Approximate equilibrium of iAs^V adsorption was shown to occur at 24 hours. The adsorption isotherm of iAs^V plotted as the percent arsenic adsorbed versus time is shown in Figure 12. Comparison of the endmember concentrations shows that at 1 hour, percent adsorption of iAs^V at an initial concentration of 0.09 µM (55.3%) was similar to the percent adsorption of iAs^V at an initial concentration of 8.7 µM (54.0%). At the lower

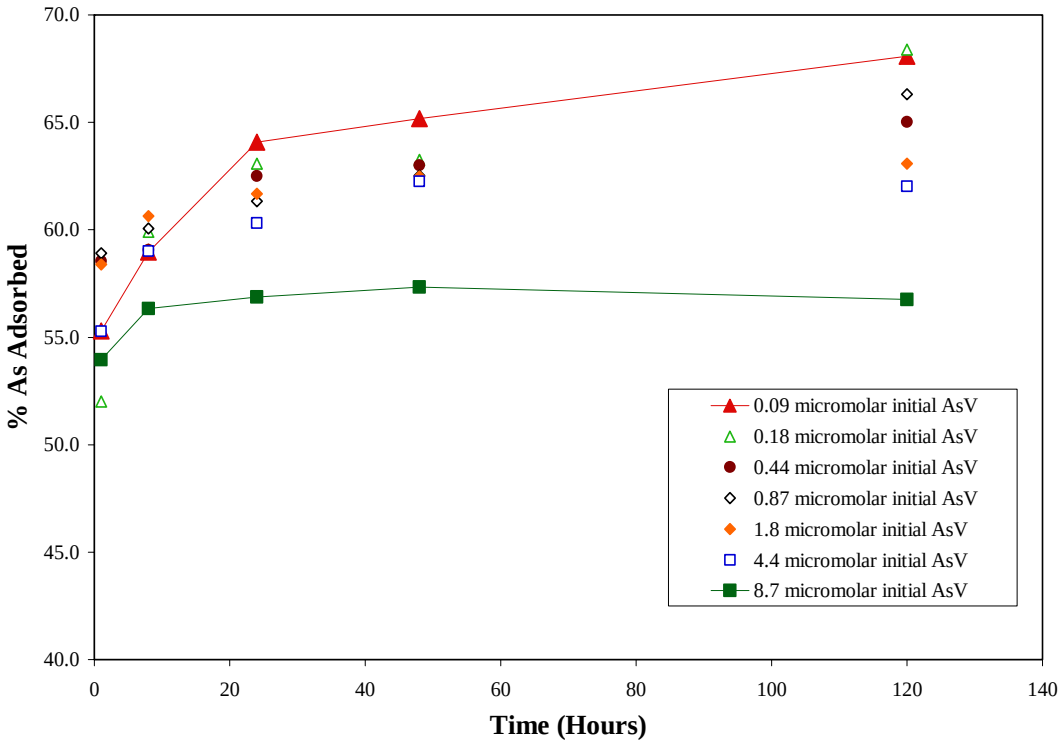

Figure 12. Adsorption kinetics for iAs^V at seven different concentrations plotted as the percent of arsenic adsorbed versus time.

concentration (0.09 µM), adsorption continued to increase up to 120 hours (from 55% to 68%). At the higher concentration (8.7 µM), adsorption increased up to 8 hours (from 54% to 57%) and then remained relatively constant thereafter. Across the entire range of initial arsenic concentration, the initial iAs^V adsorption reaction was relatively rapid;

however, the final approach to equilibrium appeared to be slower with decreasing initial As concentration. The final proportion of adsorbed iAs^V was greater at the lowest initial dissolved As concentration.

Kinetics Experiment #2. In the second series of kinetic experiments, a more rigorous evaluation of iAs^V adsorption as a function of time was performed at both a high and low initial concentration of iAs^V (4.4 µM and 263 µM). The reaction at both concentrations was monitored at times of 1, 2, 5, 10, 20, 30, 40, 50, 60, 120, 180, 240,

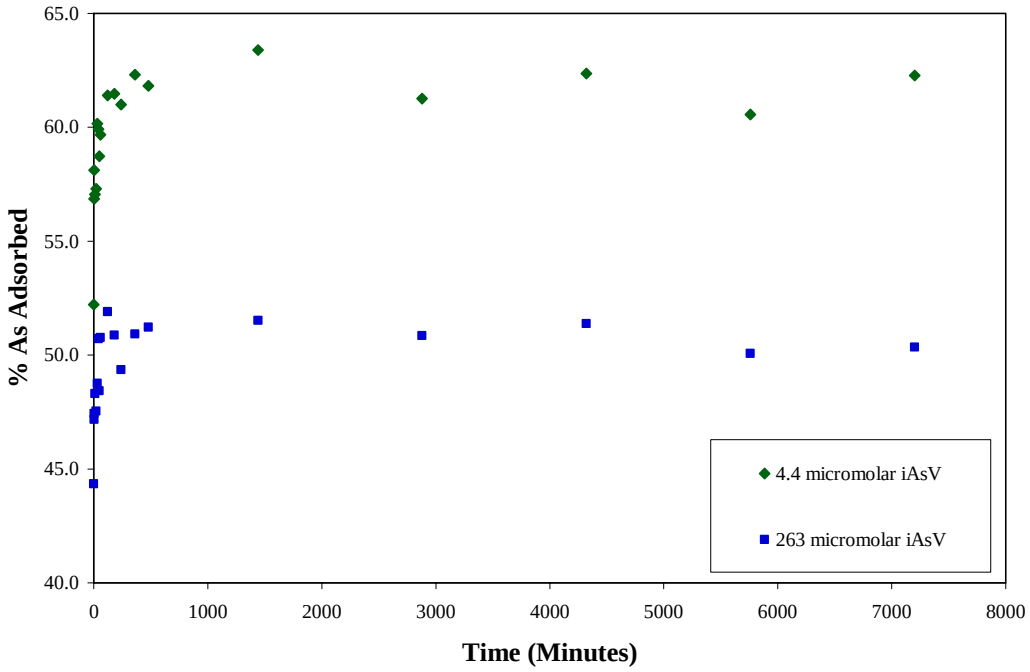

Figure 13. Adsorption kinetics at 4.4 and 263 µM iAs^V concentrations plotted as the percent of arsenic adsorbed versus time over a 5-day period.

360, 480, 1440, 2880, 4320, 5760 and 7200 minutes. The adsorption kinetics for iAs^V plotted as the percent of arsenic adsorbed versus time over the 5-day period is shown in

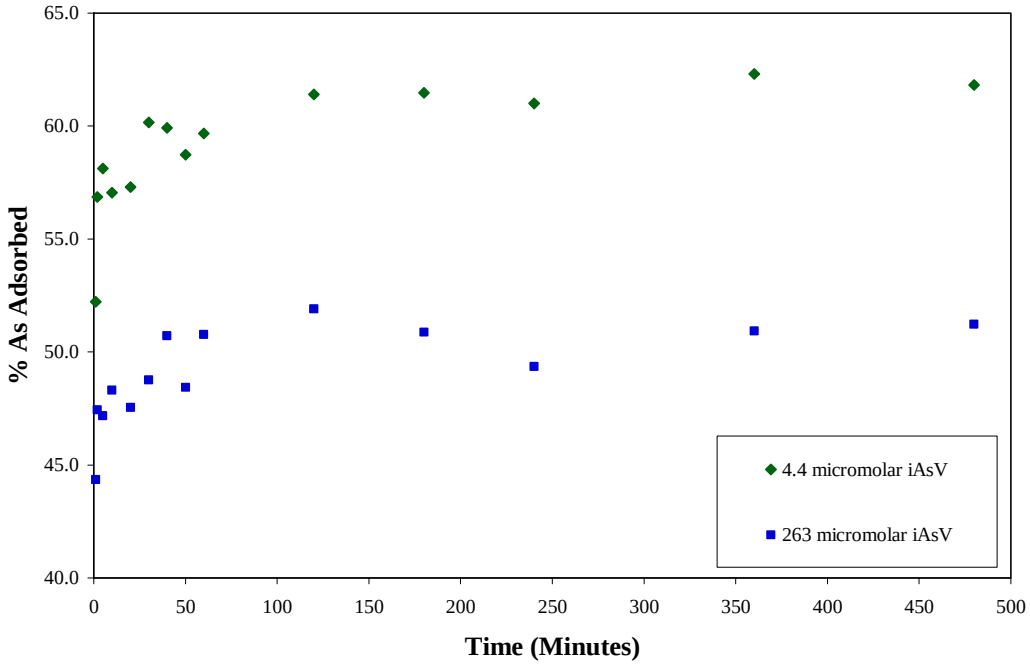

Figure 14. Adsorption kinetics at 4.4 and 263 µM iAs^V concentrations plotted as the percent of arsenic adsorbed versus time over an 8-hour interval.

Figure 13. The initial adsorption of iAs^V was relatively rapid in both cases; however, the percent of iAs^V adsorbed was substantially less at an initial concentration of 263 µM than at 4.4 µM at all measured reaction times. The adsorption of arsenic in this plot appeared to remain relatively constant after the first 8 hours of reaction with 61 – 63% of iAs^V adsorbed at 4.4 µM initial concentration and 49 – 51% of iAs^V adsorbed at 263 µM initial concentration. The adsorption kinetics for iAs^V plotted as the percent of arsenic adsorbed versus time over an 8-hour interval is shown in Figure 14. The adsorption of arsenic in this plot more clearly shows that at both initial concentrations, equilibrium was established within approximately 2 hours. Adsorbed arsenic concentrations remain relatively constant after 1 or 2 hours for the duration of the reaction of 5 days.

These results appear to demonstrate that the reaction rate is relatively fast within the first hour or two of reaction and considerably less as equilibrium is approached. The kinetics experiments have also indicated that approximate equilibrium is achieved more rapidly as the initial iAs^{V} concentration is increased. The more rapid achievement of approximate equilibrium indicates that either iAs^{V} adsorption by calcite or calcium arsenate precipitation is occurring more rapidly under this condition. In studies of the adsorption of phosphate on calcite, Celi et al. (2000) suggested that a change in mechanism from surface adsorption to surface precipitation of phosphate on calcite occurred at higher phosphate concentrations. This change in mechanism was also noted as being simultaneous with a slower reaction rate as surface precipitation became the predominant mechanism of reaction. This possible relationship between adsorbate concentration and reaction mechanism is not especially evident in the current study.

Adsorption Isotherms

Effect of Arsenic Oxidation State. For the adsorption isotherms plotted as equilibrium dissolved arsenic concentration versus mass of arsenic adsorbed, iAs^{V} was adsorbed in a greater amount than iAs^{III} at all equilibrium dissolved arsenic concentrations (Figure 15). When the adsorption isotherm was plotted as the percent of arsenic adsorbed versus initial concentration of arsenic, the adsorption of iAs^{V} was greater than 80% compared to 50% for iAs^{III} at < 10 µM initial arsenic concentrations (Figure 16). As the initial concentration of both iAs^{V} and iAs^{III} increased to more than 250 µM initial concentrations, the percent of iAs^{V} and iAs^{III} adsorbed converged to within 5.8%.

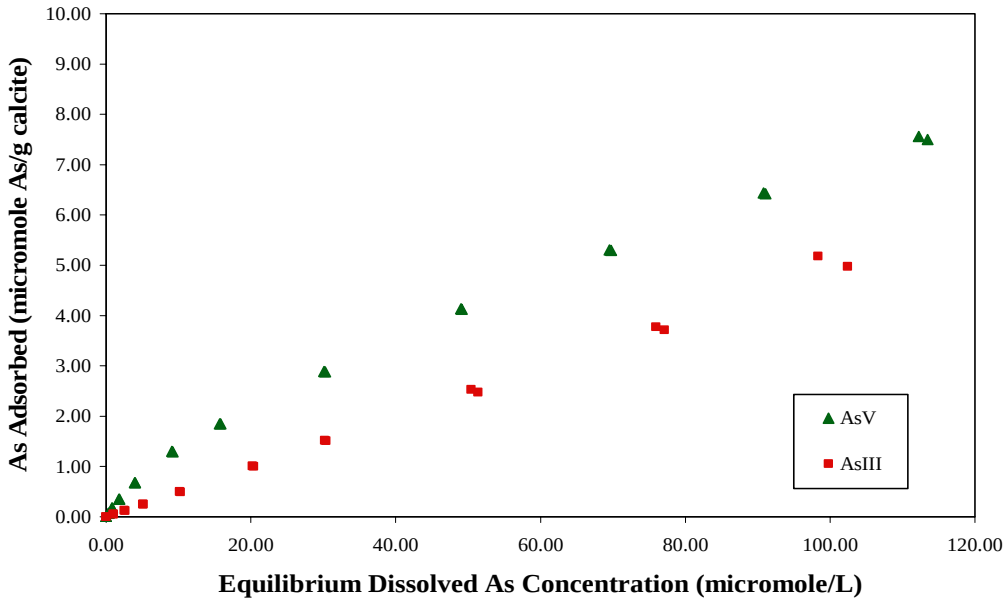

Figure 15. Adsorption isotherms for iAs^{V} and iAs^{III} plotted as the mass of arsenic adsorbed versus equilibrium dissolved arsenic concentration.

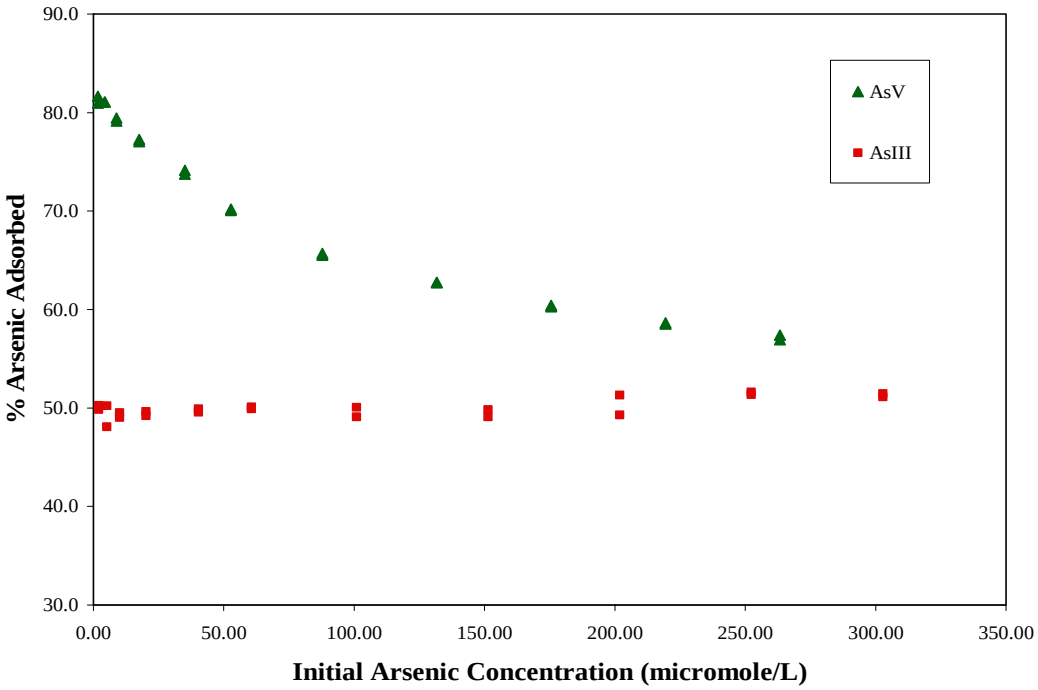

Figure 16. Adsorption isotherms for iAs^{V} and iAs^{III} plotted as the percent of arsenic adsorbed versus initial arsenic concentration.

The differences in adsorption behavior of iAs^{V} and iAs^{III} are shown in Figure 16 with much greater difference in adsorption at low concentrations and similar adsorption at higher concentrations. The adsorption behavior of iAs^{III} does not seem to exhibit the dual mechanism behavior as proposed for iAs^{V} (i.e. surface adsorption being the primary mechanism at low concentrations and surface precipitation at higher concentrations). The adsorption of iAs^{III} seems to indicate the possibility of precipitation across the entire range of initial arsenic concentrations. Formation constants for Ca-iAs^{III} solid phases could elucidate the possible mechanism, although this information is not currently available. Based on the studies by Bothe and Brown (1999a), the solid phases of iAs^{V} most likely to form (at high concentrations of iAs^{V}) at the experimental pH of 8.0 are $Ca_3(AsO_4)_2 \cdot 3\,^2/_3\, H_2O$, $Ca_3(AsO_4)_2 \cdot 4\,^1/_4\, H_2O$ and $Ca_5(AsO_4)_3OH$.

The speciation of iAs^{V} and iAs^{III} at the experimental pH of approximately 8.0 could provide an explanation for the difference in adsorption behavior between the two oxidation states of arsenic. Based on the pK_a values (from Table 3; Wagman et al., 1982), iAs^{V} exists mostly as $HAsO_4^{2-}$ (and as $H_2AsO_4^{-}$ to a lesser extent) at the experimental pH. The reduced form of arsenic, i.e., iAs^{III}, would primarily exist as the neutral species $H_3AsO_3^{o}$. The calcite surface sites that are most abundant at the experimental pH are $>CaOH_2^{+}$, $>CO_3^{2-}$ and $>CO_3Ca^{+}$ (from Table 2; Fenter et al., 1999). Electrostatic attraction and adsorption of $HAsO_4^{2-}$ and $H_2AsO_4^{-}$ to the positively charged surface sites ($>CaOH_2^{+}$ and $>CO_3Ca^{+}$) would probably tend to be favored compared to that of neutral $H_3AsO_3^{o}$. The calcite surface sites that are either negatively or neutrally charged, i.e., $>CO_3^{2-}$ and $>CaHCO_3^{o}$, should not have a significant effect on electrostatic adsorption of iAs^{III} or iAs^{V}. Adsorption of iAs^{V} and iAs^{III} to surface sites might also involve H-bonding

by an outer sphere complexation mechanism.

Effect of Arsenic Methylation. For the adsorption isotherm plotted as equilibrium dissolved arsenic concentration versus the mass of arsenic adsorbed, iAs^V was adsorbed in a greater amount than either $MMAs^V$ or $DMAs^V$, while $DMAs^V$ exhibited greater adsorption than $MMAs^V$ at all equilibrium dissolved arsenic concentrations (Figure 17).

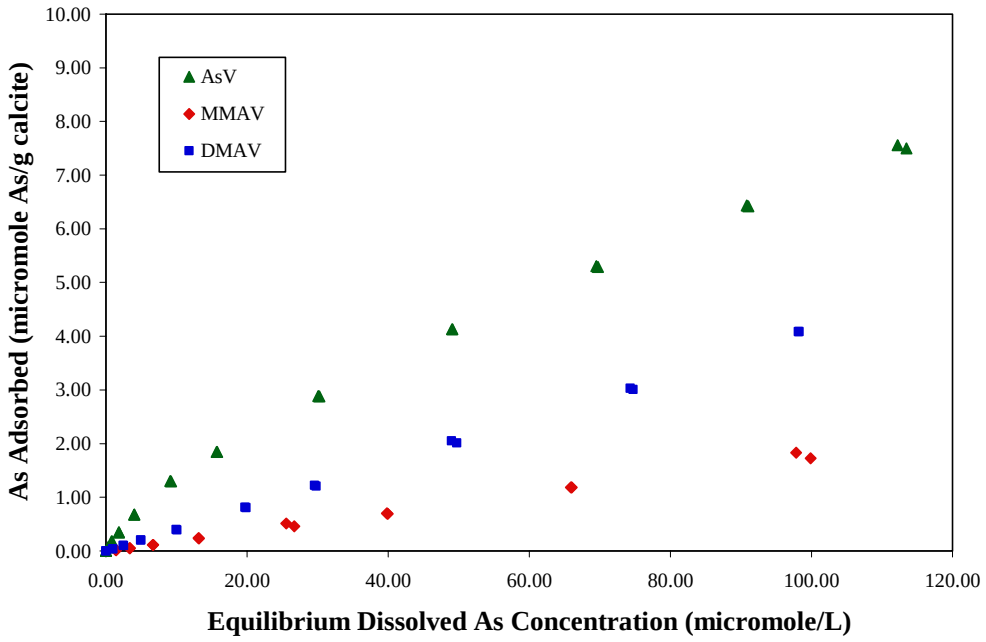

Figure 17. Adsorption isotherms for iAs^V, $MMAs^V$ and $DMAs^V$ plotted as the mass of arsenic adsorbed versus equilibrium dissolved arsenic concentration.

When the adsorption isotherm was plotted as the percent of arsenic adsorbed versus the initial concentration of arsenic, iAs^V showed a strong adsorption of greater than 80% at < 10 µM initial concentration and decreased to 57% as the initial concentration of arsenic was increased to > 250 µM (Figure 18). $DMAs^V$ demonstrated a constant adsorption of about 45% across the entire range of initial arsenic concentration. $MMAs^V$ showed an

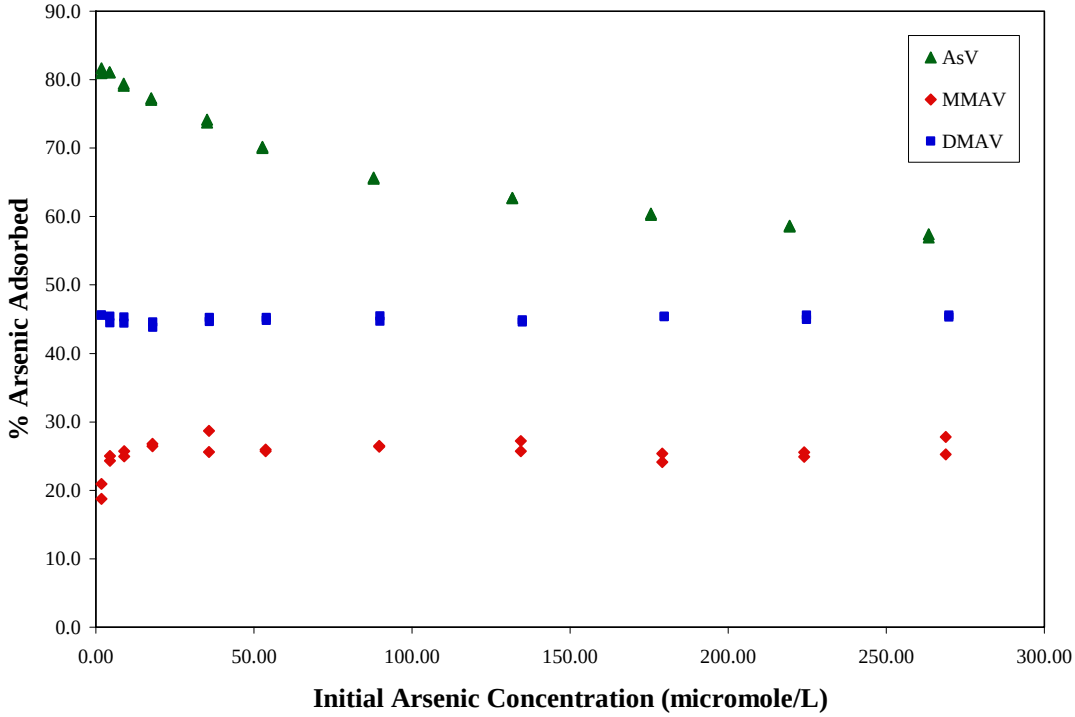

Figure 18. Adsorption isotherms for iAs^{V}, $MMAs^{V}$ and $DMAs^{V}$ plotted as the percent of arsenic adsorbed versus initial arsenic concentration.

initial increase from about 20 to 25% as the initial concentration of arsenic was increased from 1.8 µM to 4.5 µM and maintained a constant adsorption of about 25% as the initial concentration was increased to 270 µM.

The differences in the adsorption behavior of the two methylated arsenic compounds ($MMAs^{V}$, $DMAs^{V}$) and inorganic arsenic (iAs^{V}) could be at least partially attributable to differences in the protonation states of the compounds at the experimental pH of 8.0 (Table 3; Smith and Martell, 1976). $MMAs^{V}$ exists primarily as $(CH_3)HAsO_3^-$, $DMAs^{V}$ exists mostly as $(CH_3)_2AsO_2^-$, and $HAsO_4^{2-}$ is the predominant species of iAs^{V} at the experimental pH. If adsorption is impacted by electrostatic interactions with $>CaOH_2^+$ and $>CO_3Ca^+$ sites at the calcite surface, then differences in species charge could possibly

explain the greater adsorption of $HAsO_4^{2-}$ than that of the methylated arsenic compounds at low initial arsenic concentrations. The primary species of $MMAs^V$ and $DMAs^V$ at the experimental pH are both singly charged, but $DMAs^V$ exhibited a greater adsorption than $MMAs^V$ to the calcite surface across the entire range of arsenic concentrations. This difference could be due to the enhanced Van der Waals attractive forces, attributable to the additional methyl group, either at the mineral surface or in a separate precipitated solid phase.

Effect of Calcium. The adsorption behavior of iAs^V was observed under the influence of two different, initial concentrations of calcium. The adsorption of iAs^V in the 0.01 M $Ca(NO_3)_2$ equilibrated calcite suspension was adsorbed in a greater amount than

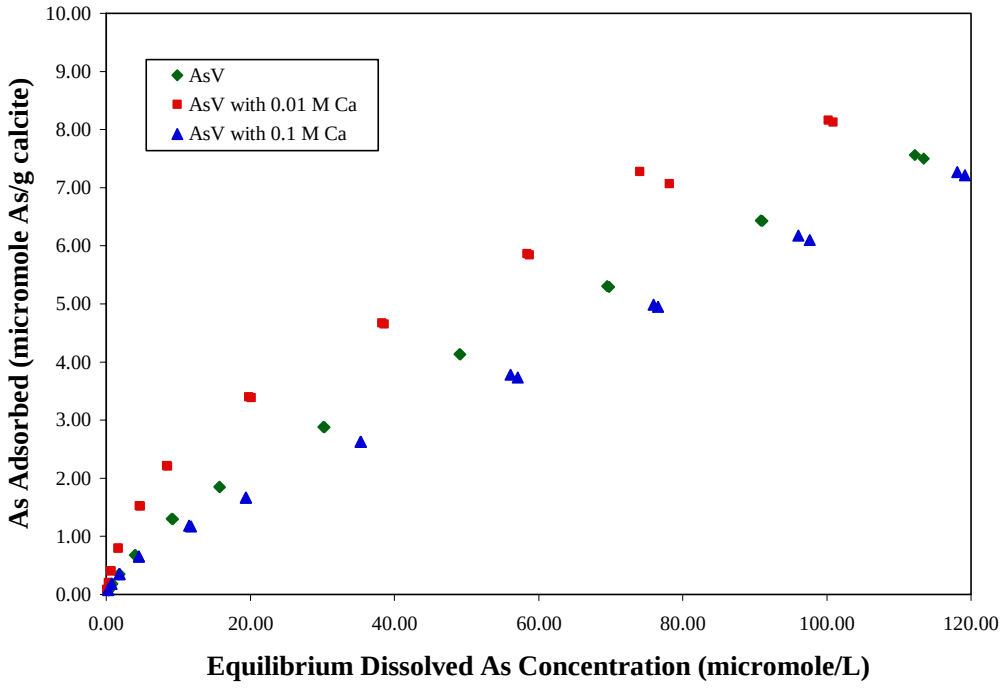

Figure 19. Adsorption isotherms for iAs^V, iAs^V with 0.01 M $Ca(NO_3)_2$ and iAs^V with 0.1 M $Ca(NO_3)_2$ plotted as the mass of arsenic adsorbed versus equilibrium dissolved arsenic concentration.

iAs^V without added initial calcium and iAs^V in the 0.1 M $Ca(NO_3)_2$ equilibrated calcite suspension. The adsorption of iAs^V in the 0.1 M $Ca(NO_3)_2$ equilibrated calcite suspension was adsorbed in a lesser amount than iAs^V without added calcium, except at equilibrium iAs^V concentrations < 1 µM where 0.1 M $Ca(NO_3)_2$ enhanced adsorption (Figure 19). When the adsorption isotherm was plotted as the percent of arsenic adsorbed versus the initial concentration of arsenic, iAs^V in the 0.01 M $Ca(NO_3)_2$ equilibrated calcite suspension showed the highest adsorption with over 92% adsorbed at < 10 µM initial arsenic concentration and 62% adsorbed as the initial arsenic concentration was increased to > 250 µM (Figure 20). The adsorption of iAs^V in the 0.1 M $Ca(NO_3)_2$ equilibrated calcite suspension decreased rapidly from 86% adsorbed at 1.8 µM initial iAs^V

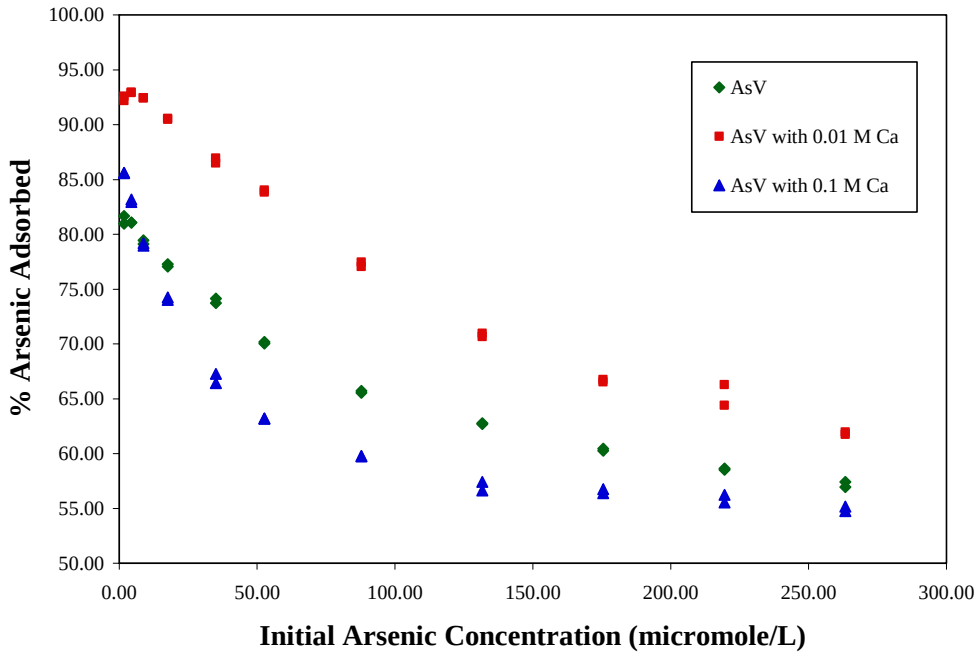

Figure 20. Adsorption isotherms for iAs^V, iAs^V with 0.01 M $Ca(NO_3)_2$ and iAs^V with 0.1 M $Ca(NO_3)_2$ plotted as the percent of arsenic adsorbed versus initial arsenic concentration.

concentration to 67% adsorbed at 35 µM initial iAs^V concentration and was greater than iAs^V without added calcium only at initial iAs^V concentrations < 5 µM. The adsorption of iAs^V without added initial calcium concentration exhibited the least adsorption of 81% at < 5 µM initial iAs^V concentration but showed a greater adsorption than the 0.1 M $Ca(NO_3)_2$ equilibrated calcite suspension as the initial iAs^V concentration was increased to > 250 µM.

The adsorption behavior of $MMAs^V$ was observed under the influence of a 0.01 M $Ca(NO_3)_2$ equilibrated calcite suspension. The adsorption isotherm plotted as equilibrium arsenic concentration versus µmoles of arsenic adsorbed is shown in Figure 21. The amount of MMA^V adsorbed was less at all equilibrium concentrations in the 0.01 M $Ca(NO_3)_2$ equilibrated calcite suspension compared to that without the addition of

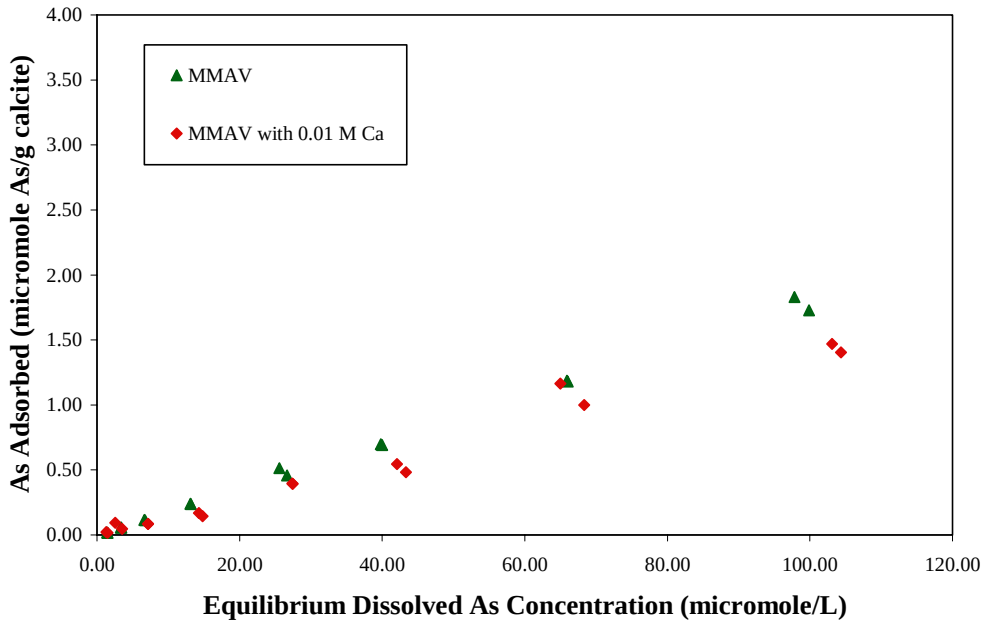

Figure 21. Adsorption isotherms for $MMAs^V$ and $MMAs^V$ with 0.01 M $Ca(NO_3)_2$ plotted as the mass of arsenic adsorbed versus equilibrium dissolved arsenic concentration.

excess calcium nitrate.

The additional calcium ions in solution could interact with the surface carbonate group of calcite, $>CO_3^{2-}$ (Table 2; Fenter et al., 1999), to create a positively charged surface site, i.e., $>CO_3Ca^+$, to which $HAsO_4^{2-}$ species could adsorb. This effect on the calcite surface could enhance the adsorption of iAs^V when surface adsorption is the primary mechanism. The increased adsorption of iAs^V (at low, initial iAs^V concentrations) with an increase in Ca^{2+} concentration could also be due to depression of the diffuse double layer thickness at the increased ionic strength, thereby allowing iAs^V to more readily enter the double layer and coordinate with surface, calcium species $>CaOH_2^+$ and $>CO_3Ca^+$. An increase from 0.01 to 0.1 M $Ca(NO_3)_2$, which resulted in a decrease in iAs^V adsorption at initial iAs^V concentrations > 5 µM, could suggest that NO_3^- was competing with iAs^V for adsorption sites. Millero et al. (2001) demonstrated that a 0.01 M Ca^{2+} concentration (the concentration present in natural seawater) increased the adsorption of phosphate on calcite by affecting the surface properties of the solid phase, although further increases in the ionic strength resulted in decreased adsorption of phosphate.

The smaller relative difference in percent iAs^V adsorbed at high initial concentrations of arsenic (Figure 20) suggests that precipitation of calcium arsenate could be less affected by NO_3^- interaction at the calcite surface and more greatly influenced by the increased molar concentration of dissolved, aqueous calcium. At high iAs^V concentrations, the most likely calcium containing solid phase to precipitate at the surface under these experimental conditions would be $Ca_3(AsO_4)_2 \cdot 3\,^2/_3\,H_2O$, $Ca_3(AsO_4)_2 \cdot 4\,^1/_4\,H_2O$ and $Ca_5(AsO_4)_3OH$ (Bothe and Brown, 1999a).

Effect of Magnesium. The adsorption characteristic of iAs^V was observed with a 0.01 M initial concentration of magnesium added to the reaction suspension. The adsorption of iAs^V without added magnesium concentration was greater extent than that of iAs^V in the 0.01 M $Mg(NO_3)_2$ equilibrated calcite suspension (Figure 22). When the

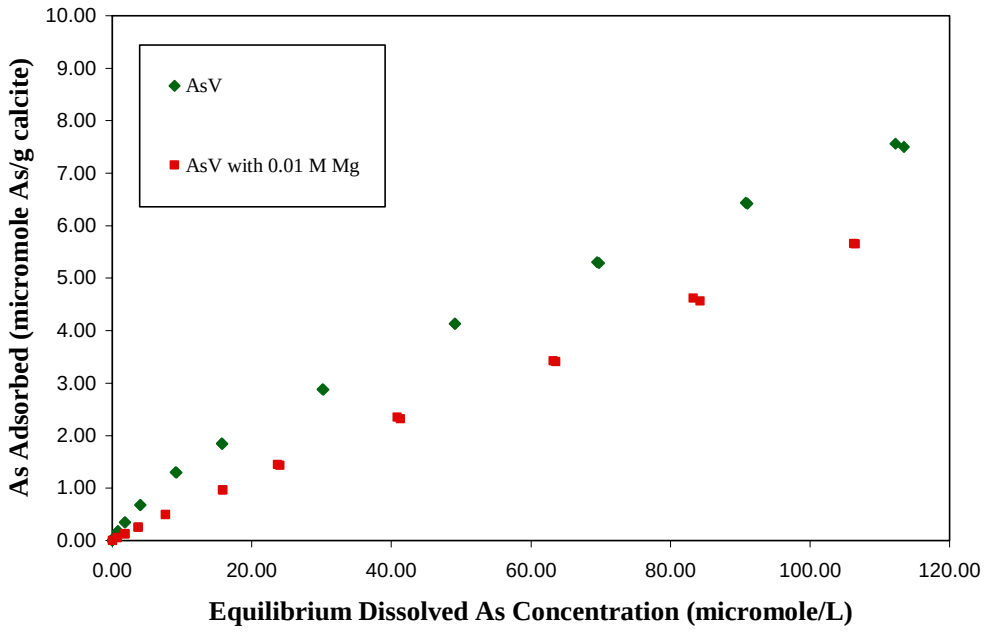

Figure 22. Adsorption isotherms for iAs^V and iAs^V with 0.01 M $Mg(NO_3)_2$ plotted as the mass of arsenic adsorbed versus equilibrium dissolved arsenic concentration.

adsorption isotherm was plotted as the percent of arsenic adsorbed versus the initial concentration of arsenic, iAs^V without added magnesium had higher adsorption at all initial concentrations of arsenic (Figure 23). The adsorption of iAs^V in the 0.01 M $Mg(NO_3)_2$ equilibrated calcite suspension exhibited a decrease in the adsorption of iAs^V from 58% to 51% as the initial concentration of iAs^V was increased from 2 µM to 263 µM.

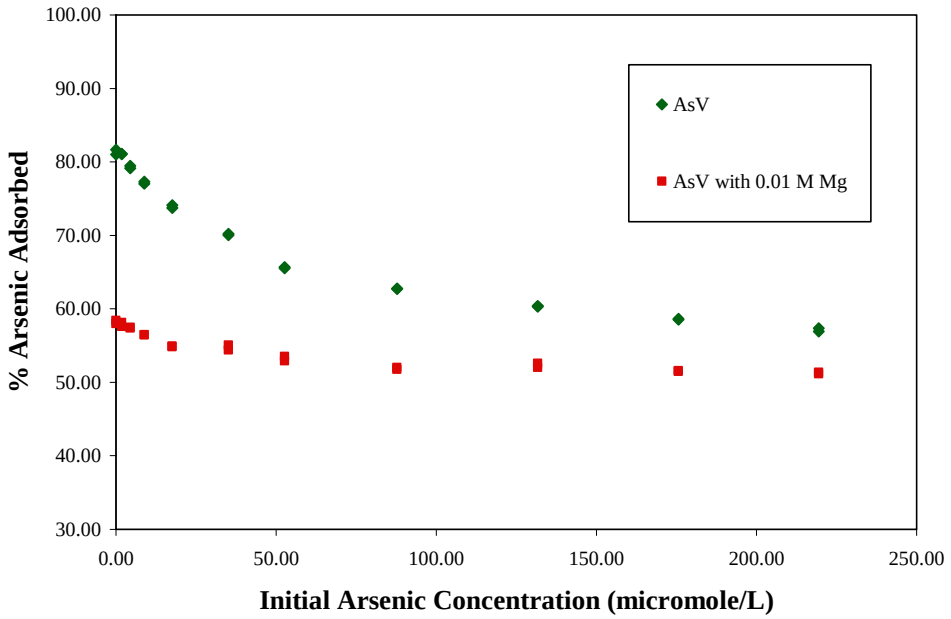

Figure 23. Adsorption isotherms for $iAs^V$and iAs^V with 0.01 M $Mg(NO_3)_2$ plotted as the percent of arsenic adsorbed versus initial arsenic concentration.

The excess dissolved magnesium at low arsenic concentrations did not enhance the surface adsorption of iAs^V as did the slight excess of dissolved calcium (Figure 20). Spectroscopic studies will be required to determine the effect of Mg^{2+} on calcite surface characteristics or the surface adsorption reaction. Adsorbed Mg^{2+} might have altered the surface properties of calcite and subsequent iAs^V adsorption as indicated by the reduced adsorption at low initial iAs^V concentration. Adsorbed Mg^{2+} is likely to be more highly hydrated than adsorbed Ca^{2+}, which would probably impact the interaction of iAs^V at the surface.

Another possible difference distinguishing the effects of calcium and magnesium could be the difference in the solubility products (K_{sp}) of calcium and magnesium

arsenate solid phases that could precipitate at the surface. The solubility products of calcium arsenate hydrates as determined by Bothe and Brown (1999b) and by Zhu et al. (2006) have pK_{sp} values which range from 21.0 to 38.0 and have slightly lower solubilities than magnesium arsenate ($Mg_3(AsO_4)_2$) which has a pK_{sp} of 19.7 (Magalhaes, 2002). The solubility of other magnesium arsenates such as Hoernisite ($Mg_3(AsO_4)_2 \cdot 8\ H_2O$) is poorly known.

Effect of Phosphate. The phosphate adsorption isotherm was evaluated under the same experimental conditions as that of iAs^V. For the adsorption isotherms plotted as mass adsorbed versus the equilibrium dissolved concentration (Figure 24), the amount of P adsorbed per gram of calcite was considerably higher than the amount of iAs^V adsorbed at equilibrium concentrations < 70 µM. The amount of iAs^V adsorbed was higher than P

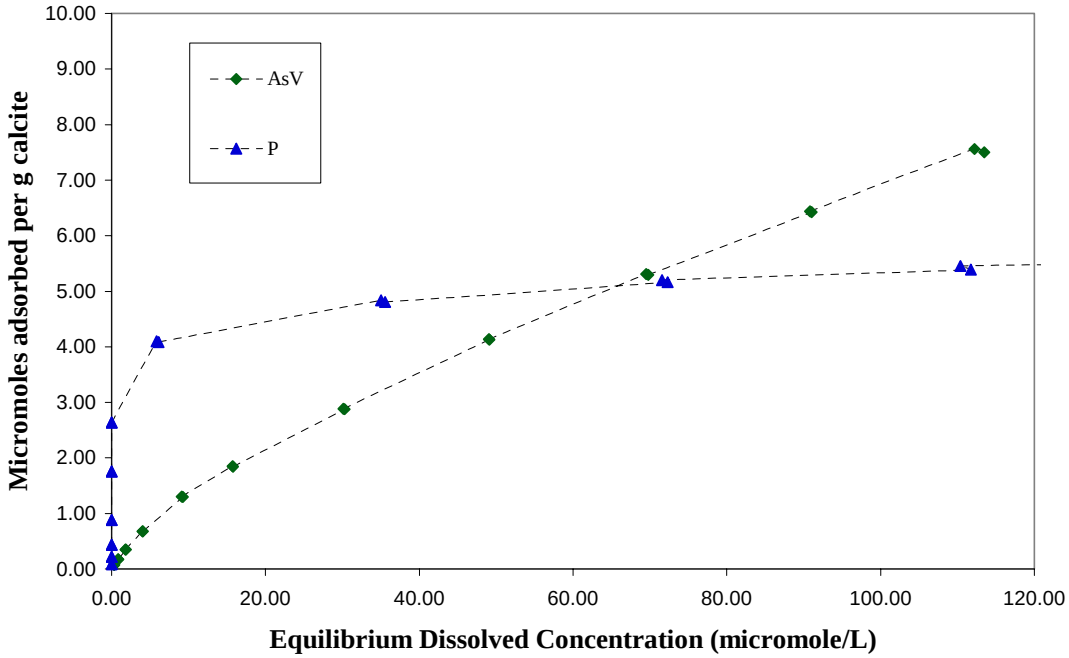

Figure 24. Adsorption isotherms for P and iAs^V plotted as the mass adsorbed versus equilibrium dissolved concentration.

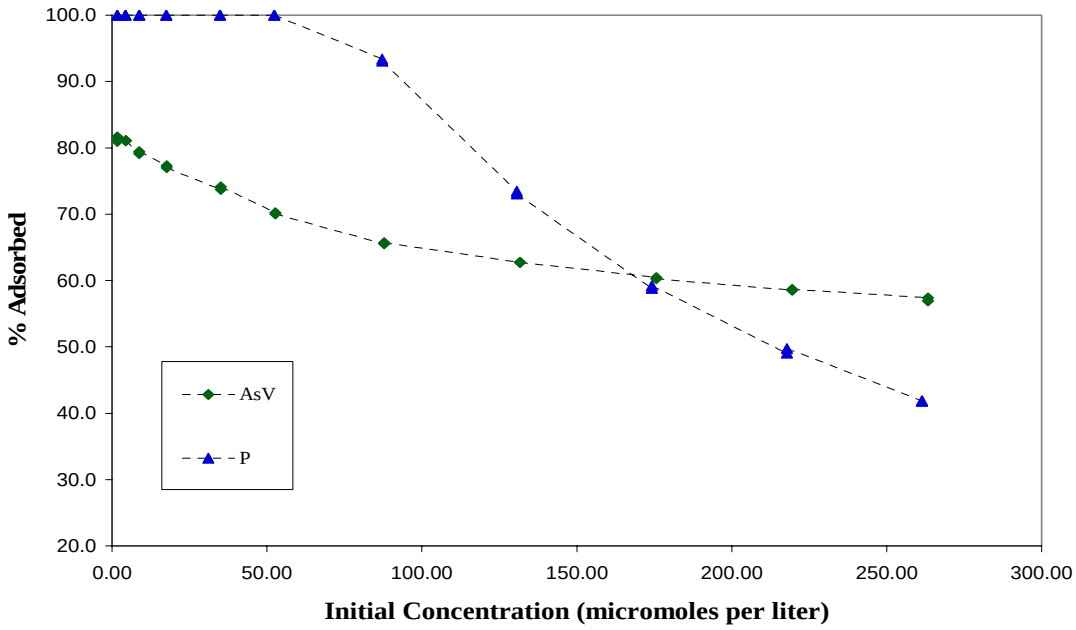

Figure 25. Adsorption isotherms for P and iAs^V plotted as the percent adsorbed versus initial concentration.

at equilibrium concentrations > 70 µM. For the adsorption isotherms plotted as percent adsorbed versus the initial concentration (Figure 25), the concentration of P in solution was not detectable (100% adsorption) until the initial concentration was > 80 µM. The percent adsorption of phosphate was greater than that of iAs^V at initial concentrations < 170 µM but less than that of iAs^V at initial concentrations > 170 µM. The maximum initial concentration of dissolved phosphate was 260 µM, which resulted in 42 % adsorption of P while the adsorption of iAs^V at this concentration was 57%. These results indicate different predominant mechanisms of iAs^V compared to phosphate adsorption at both low and high initial adsorbate concentrations.

A competitive adsorption study was performed at equimolar concentrations of P and iAs^V. The measured amount of P in solution (equilibrium concentration) in the

presence of an equimolar concentration of iAs^V was almost the same as without iAs^V and not detectable (100% adsorption) until the amount of phosphate adsorbed per gram of calcite was > 3 µmoles g^{-1} (Figure 26). At equilibrium concentrations > 6 µM, the

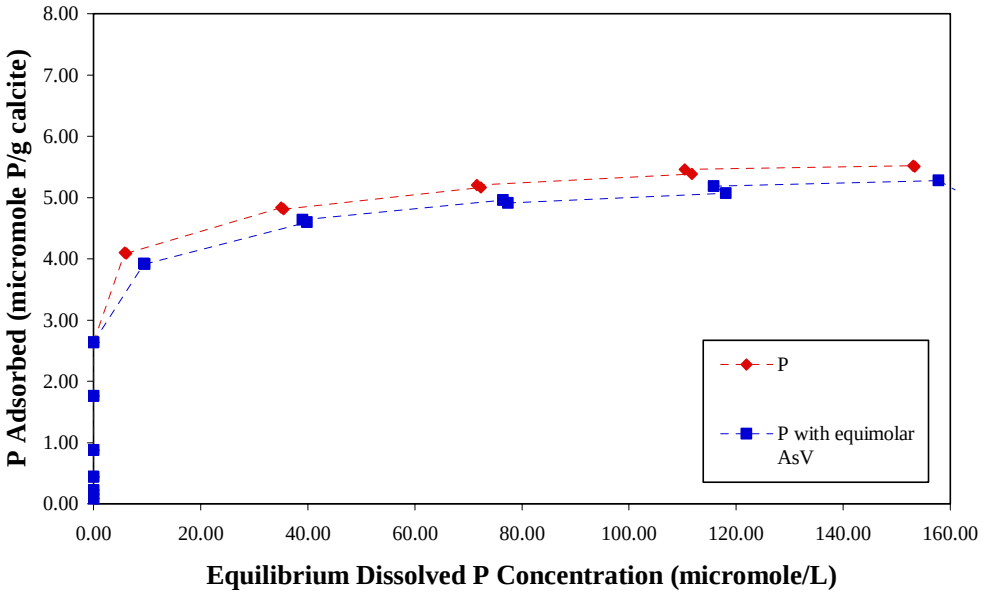

Figure 26. Adsorption isotherms for P and P with an equimolar concentration of iAs^V plotted as the mass of P adsorbed versus equilibrium dissolved P concentration.

amount of phosphate adsorbed in the presence of equimolar concentrations of iAs^V was 0.2 – 0.3 µmole per gram of calcite less than that adsorbed in the absence of iAs^V. Phosphate in both the absence and presence of iAs^V was 100% adsorbed at initial P concentrations < 52 µM (Figure 27). When the initial concentration of phosphate was increased to > 52 µM, the percent of added phosphate adsorbed in the presence of equimolar iAs^V was approximately 3% less than that adsorbed in the absence of iAs^V. The amount of iAs^V adsorbed with equimolar P was < 0.5 µmole per gram of calcite and

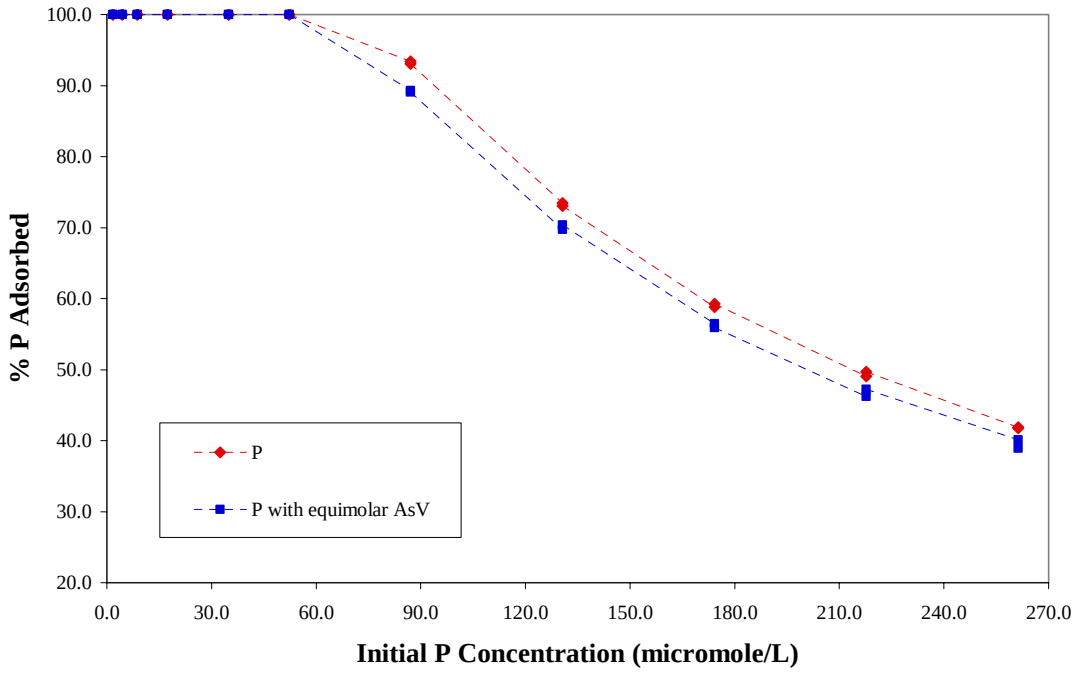

Figure 27. Adsorption isotherms for P and P with an equimolar concentration of iAs^V plotted as the percent of P adsorbed versus initial dissolved P concentration.

less than that adsorbed in the absence of iAs^V at all equilibrium concentrations (Figure 28). There was no iAs^V adsorbed in the presence of equimolar phosphate at equilibrium concentrations > 88 µM. At all initial dissolved iAs^V concentrations, the percent iAs^V adsorbed in the absence of phosphate was much greater than that adsorbed in the presence of equimolar P (Figure 29). When the initial concentration of iAs^V was < 2 µM, the percent of iAs^V adsorbed was 81% in the absence of P compared to 54% adsorption of iAs^V with equimolar P. From initial iAs^V and P concentrations of 88 µM to 263 µM, there was no adsorption of iAs^V in the presence of equimolar P.

The predominant phosphate species at pH 8.0 are HPO_4^{2-} and $H_2PO_4^-$, with the concentration of HPO_4^{2-} being much greater than that of $H_2PO_4^-$. Based on the

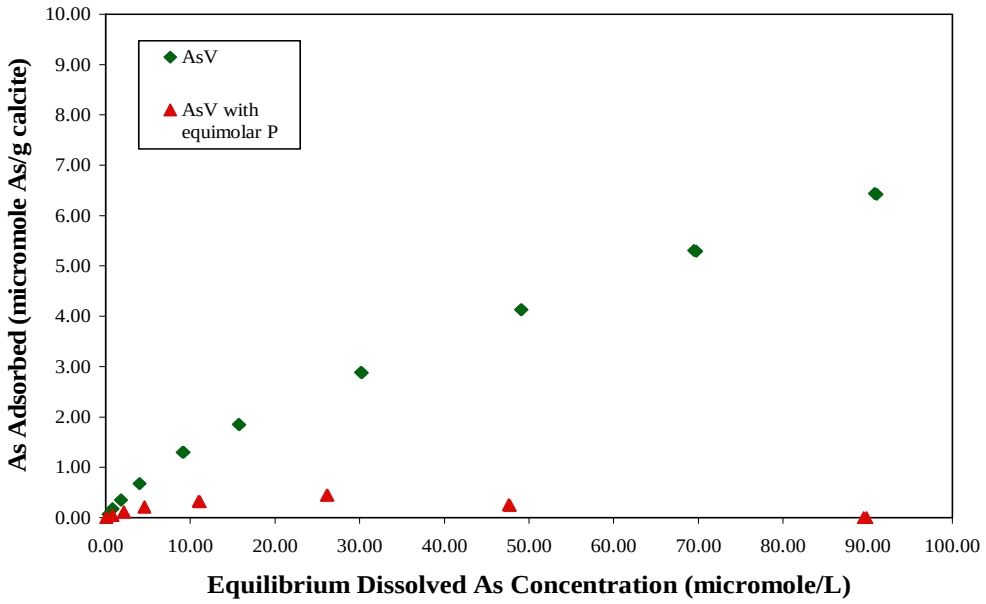

Figure 28. Adsorption isotherms for iAs^V and iAs^V with an equimolar concentration of P plotted as the mass of arsenic adsorbed versus equilibrium dissolved arsenic concentration.

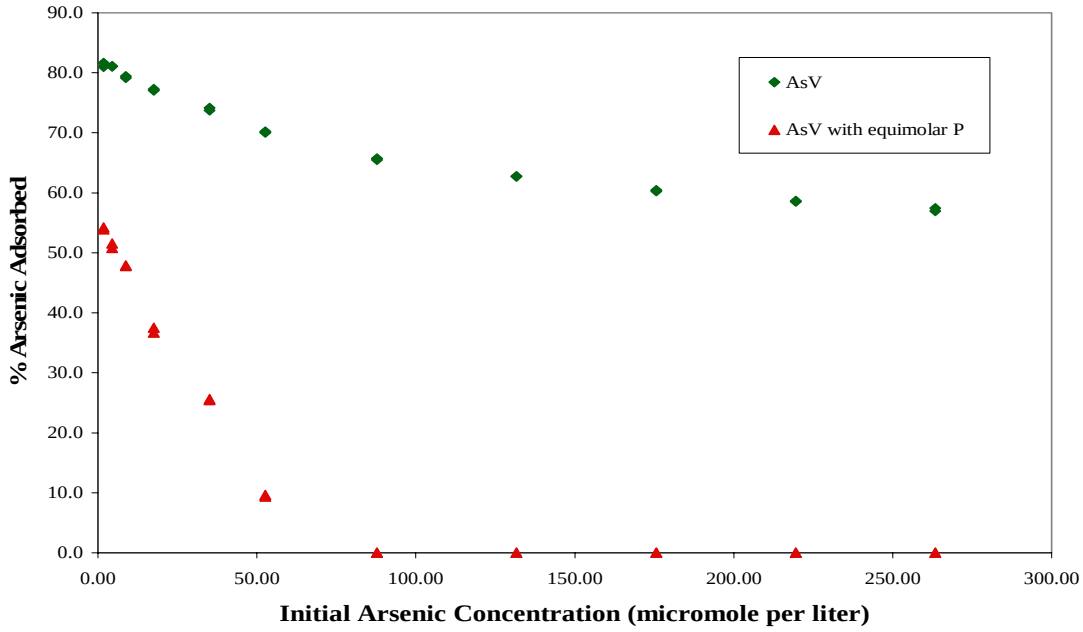

Figure 29. Adsorption isotherms for iAs^V and iAs^V with an equimolar concentration of P plotted as the percent of arsenic adsorbed versus initial arsenic concentration.

concentrations of Ca^{2+} and P in solution, $CaHPO_4^o$ and $CaPO_4^-$ (along with HPO_4^{2-} and $H_2PO_4^-$) might be important solution species that could interact with the surface of calcite (Lindsay, 1979).

Surface adsorption of HPO_4^{2-} was much greater than that of $HAsO_4^{2-}$ at low, initial, equimolar concentrations of arsenate and phosphate (Figure 27 and Figure 29). Adsorption, as opposed to precipitation, of phosphate at low concentrations was suggested by Matar et al. (1992) to occur by replacement of water molecules and direct interaction with Ca^{2+} at the surface of calcite. Based on the X-ray reflectivity data of Fenter et al. (1999), the calcite surface site most abundant at the experimental pH and able to interact by this mechanism would be $>CaOH_2^+$.

The selective adsorption of P over iAs^V at equimolar, equilibrium concentrations < 48 µM and equimolar, initial concentrations > 88 µM could be due to the consumption of available calcite surface sites by reaction with phosphate. It has been proposed that at higher concentrations of phosphate, excess HPO_4^{2-} continues to react at the calcite surface to form ion clusters, and the adsorption reaction of these ions at higher concentrations changes to a mechanism of surface precipitation and the formation of calcium phosphate phases (Celi et al., 2000). The calcium phosphate phases that can form at higher concentrations of phosphate are as follows in order of decreasing solubility (Lindsay, 1979; Brady and Weil, 2002): $Ca(H_2PO_4)_2 \cdot H_2O$ (monocalcium phosphate) > $CaHPO_4 \cdot 2\ H_2O$ (dicalcium phosphate) > $Ca_8H_2(PO_4)_6 \cdot 5\ H_2O$ (octacalcium phosphate) > $Ca_3(PO_4)_2$ (tricalcium phosphate) > $3[Ca_3(PO_4)_2] \cdot CaO$ (oxy apatite) > $3[Ca_3(PO_4)_2] \cdot Ca(OH)_2$ (hydroxy apatite) > $3[Ca_3(PO_4)_2] \cdot CaCO_3$ (carbonate apatite).

In the previous studies by Celi et al. (2000) using Fourier-transform infrared

spectroscopy (FT-IR) and laser doppler velocimetry - photon correlation spectroscopy (LDV-PCS) it was suggested that this change in mechanism from adsorption to surface precipitation occurred at an equilibrium phosphate concentration greater than 600 µM (for calcite with 2 µm mean particle diameter and 2.8 m^2 g^{-1} specific surface area), although the sorption process is specifically related to calcite surface area and particle size (Amer et al., 1985). The mean particle diameter of calcite used in these studies is 6 µm and the specific surface area is 0.2 m^2 g^{-1} as determined by Lee et al. (2005). These calcite characteristics yield a lower surface area for adsorption and a lower concentration for which the mechanism could change from surface adsorption to precipitation. Based on a qualitative interpretation of the results of these experiments, this phenomenon could be occurring at equimolar, equilibrium concentrations > 48 µM and equimolar, initial concentrations > 88 µM.

Effect of Sulfate. A competitive adsorption study was performed at equimolar concentrations of sulfate and iAs^V. For the adsorption isotherms plotted as the mass of arsenic adsorbed versus equilibrium dissolved arsenic concentration, sulfate dramatically reduced the amount of iAs^V adsorbed to < 1 µmole of iAs^V per gram of calcite at all equilibrium concentrations (Figure 30). The amount of adsorption slowly increased from 0.01 µmoles g^{-1} at 1.5 µM equilibrium iAs^V concentration to 0.70 µmoles g^{-1} at 250 equilibrium iAs^V concentration. For the adsorption isotherms plotted as the percent of arsenic adsorbed versus the initial concentration of arsenic (Figure 31), iAs^V adsorption in the presence of equimolar S was reduced from 81 to 22% at 4.4 µM initial arsenic concentration and then decreased to 7.6% adsorption at 88 µM initial concentration. From initial concentrations of 88 µM to 263µM , the percent adsorption had only a slight

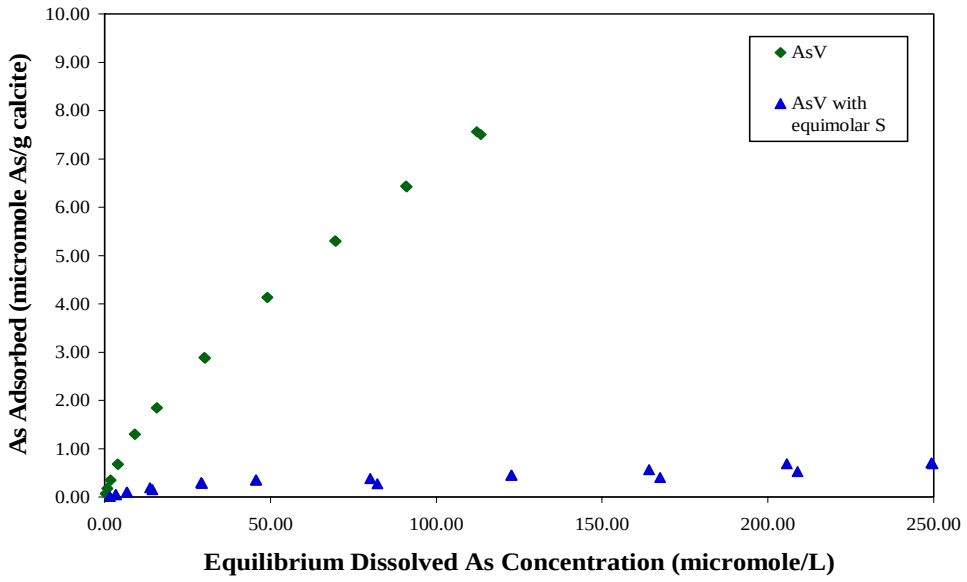

Figure 30. Adsorption isotherms for iAs^V and iAs^V with an equimolar concentration of S, as sulfate, plotted as the mass of arsenic adsorbed versus equilibrium dissolved arsenic concentration.

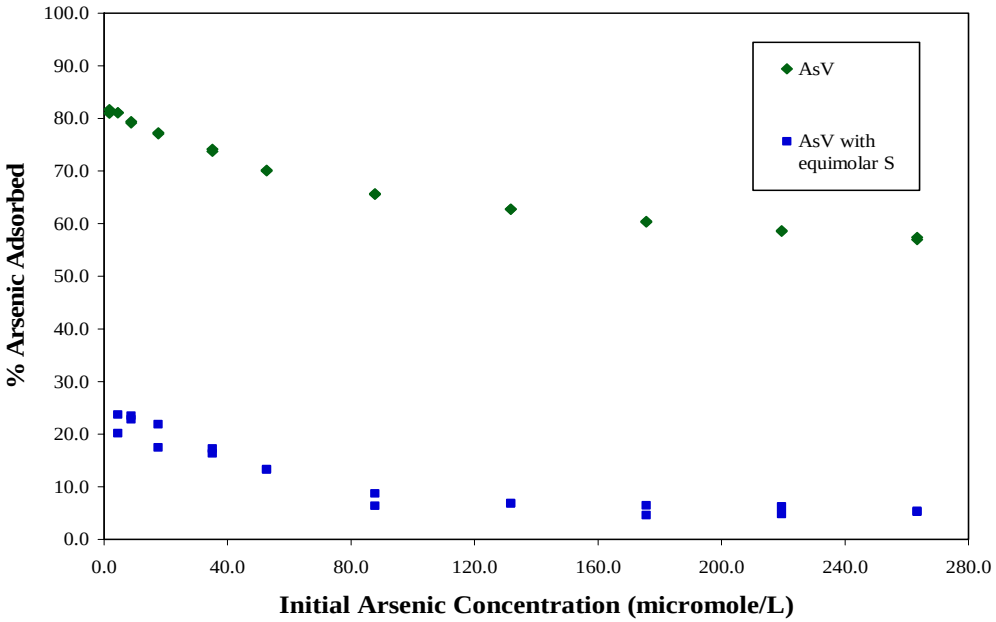

Figure 31. Adsorption isotherms for iAs^V and iAs^V with an equimolar concentration of S, as sulfate, plotted as the percent of arsenic adsorbed versus initial arsenic concentration.

further decrease from 6.9 – 5.3%.

The primary sulfate species at pH of 8.0 is SO_4^{2-}. Sulfate was shown in previous studies by Millero et al. (2001) to decrease the adsorption of phosphate. Based on the results in this study, equimolar SO_4^{2-} had a similar effect on the adsorption of iAs^V by dramatically reducing the adsorption across the full range of concentrations, although sulfate did not totally prevent the adsorption of iAs^V at high concentrations as did phosphate.

As noted previously, Matar et al. (1992) suggested that phosphate bonded directly with Ca^{2+} at the surface of calcite by forming $>Ca—PO_4$ bonds by a mechanism in which water is displaced from $>CaOH_2^+$ surface sites. The preferential adsorption of phosphate when present at equimolar concentrations of arsenic could suggest that iAs^V may not be similarly bound to the surface of calcite. The formation of water-bridged complexes with iAs^V and sulfate (i.e., $>Ca—OH_2—AsO_4$ and $>Ca—OH_2—SO_4$) might explain the inability of sulfate from excluding arsenic adsorption at higher concentrations as did phosphate. The bond strength of these water-bridged complexes would be less than that of a complex formed by direct bonding to $>Ca^{2+}$ surface sites and would allow greater ease of anion displacement.

Modeling of Adsorption Isotherms

Adsorption using the Freundlich Model versus the Langmuir Model. The adsorption of iAs^V on synthetic calcite was modeled using both the Freundlich and Langmuir equations with parameters calculated from the regression analysis of the linear form of each equation. The plot of each model with the experimental data is represented

Table 5. Freundlich equation constants (K_f and n) and coefficients of determination (R^2).

Constants and coefficients are for applicable species as derived from the regression analysis of the linear form of the Freundlich equation: $\log q = \log K_f + n \log C_{eq}$, in which q represents the amount of material adsorbed per amount of adsorbate, C_{eq} is the concentration of adsorbate at equilibrium in solution, and K_f and n are constants.

Molecular Species	K_f	n	R^2
iAs^V with synthetic calcite (lot A)	0.2042	0.777	0.997
iAs^V with ground, natural calcite	0.0612	0.950	1.000
iAs^{III}	0.0483	1.011	1.000
DMA^V	0.0408	1.001	1.000
MMA^V	0.0147	1.041	0.997
iAs^V with 0.01 M Ca^{2+}	0.4519	0.658	0.985
iAs^V with 0.1 M Ca^{2+}	0.2118	0.724	0.998
iAs^V with 0.01 M Mg^{2+}	0.1483	0.955	1.000
MMA^V with 0.01 M Ca^{2+}	0.0150	0.974	0.974
P	3.4670	0.094	0.999

Table 6. Langmuir equation constants (K_L and b) and coefficients of determination (R^2).

Constants and coefficients are for applicable species as derived from the regression analysis of the linear form of the Langmuir equation: $C_{eq} / q = (1 / bK_L) + (C_{eq} / b)$, in which q represents the amount of material adsorbed per amount of adsorbate, C_{eq} is the equilibrium concentration of adsorbent in solution, b is the adsorption maximum and K_L is the adsorption constant. Note: The symbol (-) represents irrelevant data.

Molecular Species	K_L	b	R^2
iAs^V	0.0160	10.638	0.913
iAs^{III}	-	-	0.042
MMA^V	-	-	0.024
DMA^V	-	-	0.068
P	1.2365	5.4645	0.997

in Figure 32. The Freundlich constants, K_f and n, and the coefficients of determination, R^2, are summarized in Table 5. The Langmuir constants, K_L and b, and the coefficients of determination, R^2, are summarized in Table 6. The R^2 values for the Freundlich and

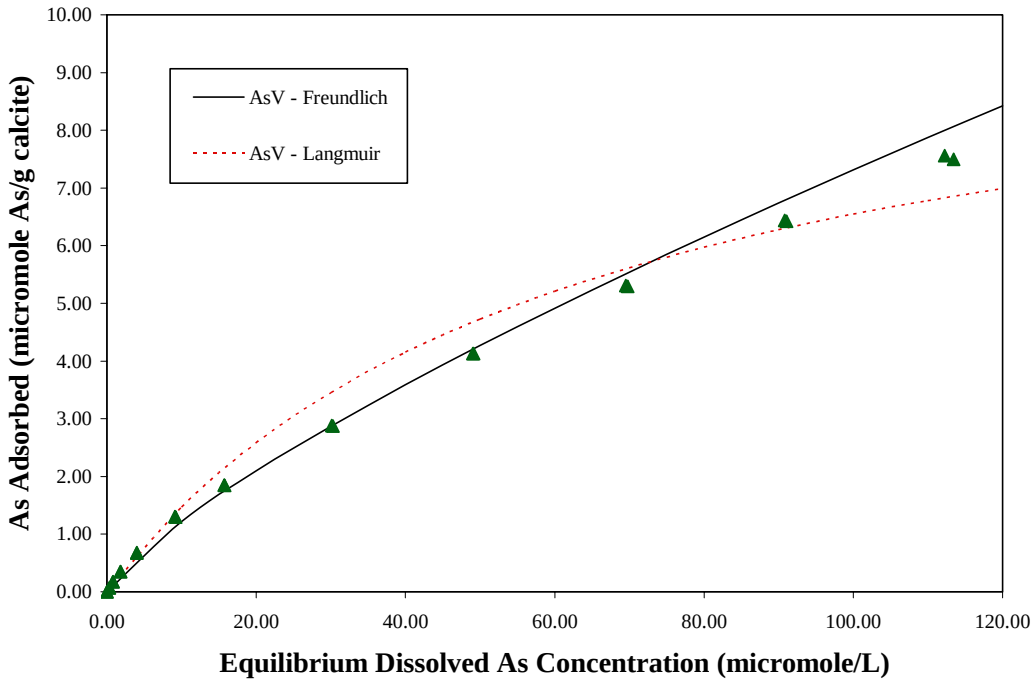

Figure 32. Adsorption isotherm for iAs^V by synthetic calcite with experimental data points and the Freundlich and Langmuir models represented by the curves.

Langmuir models were 0.997 and 0.913, respectively. The Freundlich model was more effective in describing the adsorption behavior than was the Langmuir model, as illustrated in Figure 32. The Langmuir adsorption model was theoretically derived to describe adsorption where an adsorption maximum is achieved, whereas the Freundlich model is empirical and shows a better fit of the experimental data since an adsorption maximum was not achieved during arsenic adsorption. Unless otherwise noted in this study, the adsorption of arsenic on calcite was described using the Freundlich model.

Adsorption of iAs^V on Natural Calcite versus Synthetic Calcite. The adsorption of iAs^V on synthetic and natural calcite were described using the Freundlich model, and

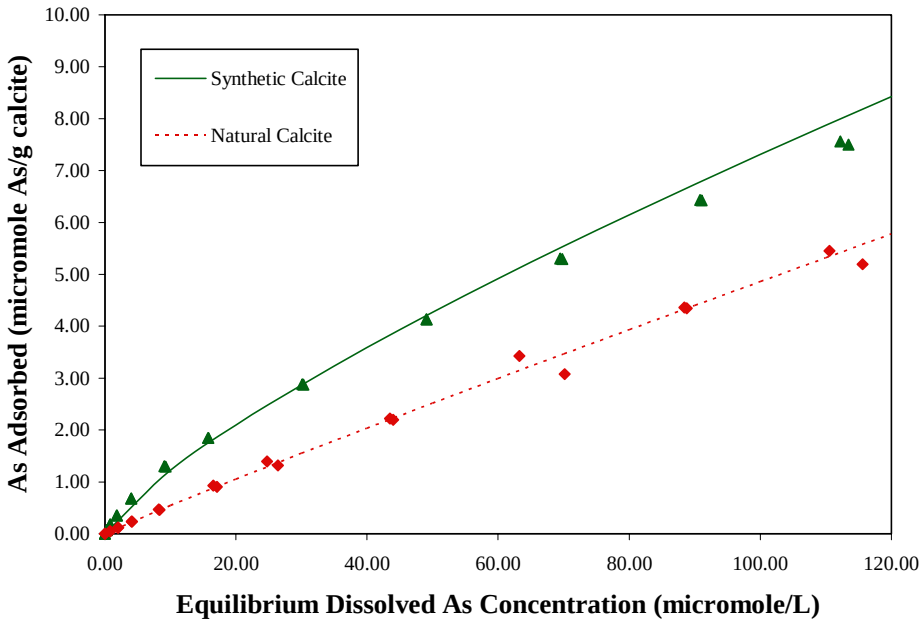

Figure 33. Adsorption isotherms for iAs^V by natural calcite and synthetic calcite with experimental data points, and the model fit represented by the curve.

plots of the models and experimental data points are shown in Figure 33. The coefficient of determination, R^2, and the Freundlich constants, K_f and n, are given in Table 5. The higher K_f value for the adsorption on synthetic calcite is indicative of higher adsorption of iAs^V at low equilibrium dissolved arsenic concentrations. The model fit for the adsorption of iAs^V on synthetic and natural calcite, as represented by the coefficients of determination, demonstrate a strong linear relationship between log C_{eq} and log q, although the model has a slightly better predictability for natural calcite with an R^2 of 1.000 than for synthetic calcite with an R^2 of 0.997.

Adsorption of iAs^{V}, iAs^{III}, DMA^{V} and MMA^{V} on Calcite. The adsorption of iAs^{V}, iAs^{III}, MMA^{V} and DMA^{V} on synthetic calcite were described using the Freundlich model, and the plots of the models and experimental data points are represented in Figure 34.

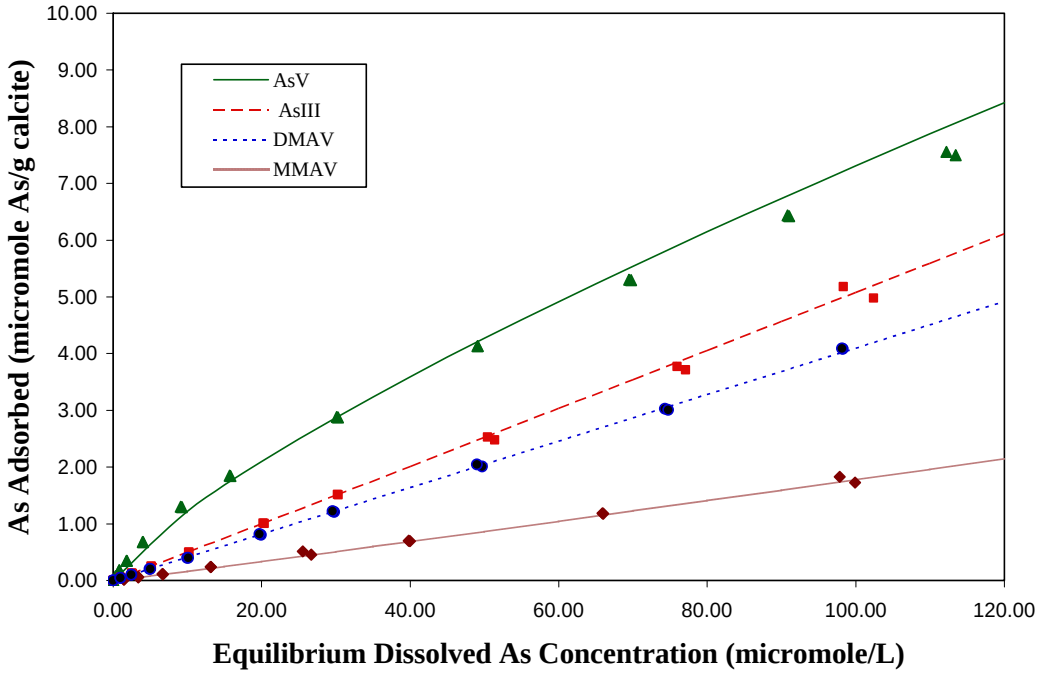

Figure 34. Adsorption isotherms for iAs^{V}, As^{III}, MMA^{V} and DMA^{V} with experimental data points, and the model fit represented by the curve.

The Freundlich constants and coefficients of determination for these adsorption isotherms are given in Table 5. The adsorption of each of these species was well described by the Freundlich model with coefficients of determination > 0.997. The adsorption of iAs^{III}, DMA^{V} and MMA^{V} was approximately linear across the range of equilibrium concentrations as shown with model values of n close to 1.000. The K_f values, which represent the strength of adsorption, decrease in the following order: iAs^{V} > iAs^{III} > DMA^{V} > MMA^{V}. The difference in the K_f values of iAs^{V} (0.2042) and MMA^{V} (0.0147)

represents an order of magnitude. This indicates that the initial adsorption of arsenic to calcite, as iAs^{V} is methylated to MMA^{V}, is decreased by a factor of approximately 0.1. The K_f values for iAs^{III} and DMA^{V} (0.0483 and 0.0418, respectively) show that the initial arsenic adsorption is decreased by a factor of approximately 0.75 when iAs^{V} is reduced to iAs^{III} or methylated to DMA^{V}.

Adsorption of iAs^{V} on Calcite with 0.01 and 0.1 M Calcium Nitrate. The adsorption of iAs^{V} on synthetic calcite as influenced by 0.01 and 0.1 M calcium nitrate was fit using the Freundlich model, and the plots of the models and experimental data points are represented in Figure 35. The Freundlich constants and coefficients of

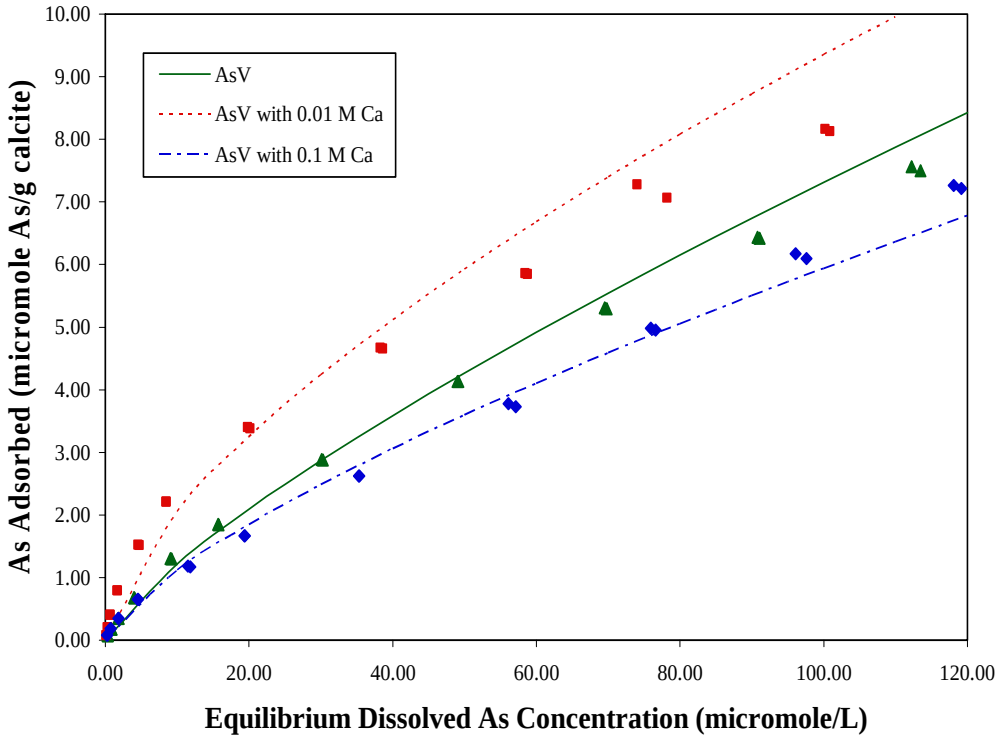

Figure 35. Adsorption isotherms for iAs^{V}, iAs^{V} with 0.01 M Ca^{2+} and iAs^{V} with 0.1 M Ca^{2+} with experimental data points, and the model fit represented by the curve.

determination are given in Table 5. The K_f values show that adsorption was greater for iAs^V with 0.01 M calcium nitrate (0.4519) than iAs^V with 0.1 M calcium nitrate (0.2118) and iAs^V without added calcium nitrate (0.2042). The similar K_f values for iAs^V with 0.1 M calcium nitrate compared to that of iAs^V without added calcium nitrate reflects similar adsorption behavior at low equilibrium arsenic concentrations. At high equilibrium arsenic concentrations, the adsorption of iAs^V without added calcium nitrate was greater than that of iAs^V with 0.1 M calcium nitrate, as indicated by a slightly higher n value which is indicative of a less concave function. The K_f value for iAs^V with 0.01 M calcium nitrate was more than twice that of iAs^V without added calcium nitrate, and suggests that the addition of 0.01 M calcium nitrate had a strong impact on the adsorption of arsenic at low equilibrium concentrations.

Adsorption of $MMAs^V$ on Calcite with 0.01 M Calcium Nitrate. The adsorption of MMA^V on synthetic calcite was fit using the Freundlich model and the plot of the model with experimental data points is represented in Figure 36. The almost identical K_f values for MMA^V in the absence and presence of 0.01 M calcium nitrate reflect the similar adsorption behavior at equilibrium concentrations < 5 µM. At the high As concentrations, the adsorption of MMA^V with 0.01 M calcium nitrate was less than that of MMA^V without added calcium nitrate, which was reflected in the slightly lower value of n.

Adsorption of iAs^V on Calcite with 0.01 M Magnesium Nitrate. The adsorption of iAs^V on calcite with 0.01 M magnesium nitrate and without added magnesium nitrate was described using the Freundlich model, and plots of the models with experimental data points are represented in Figure 37. The Freundlich parameters are given in Table 5. The model value of n (0.955) for iAs^V adsorption with 0.01 M magnesium nitrate is close to

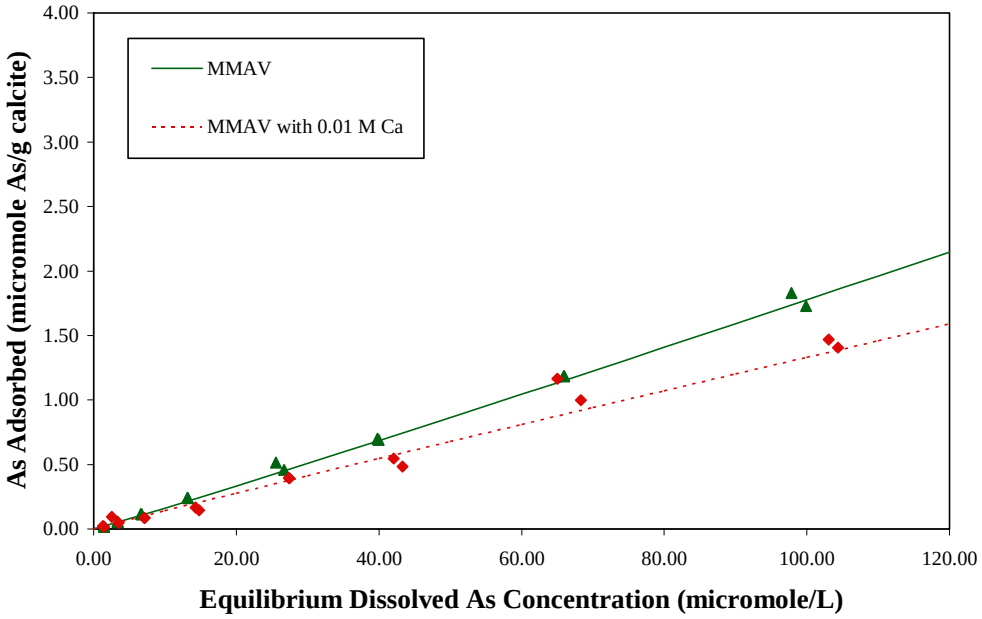

Figure 36. Adsorption isotherms for $MMAs^{V}$ and $MMAs^{V}$ with 0.01 M Ca^{2+} with experimental data points, and the model fit represented by the curve.

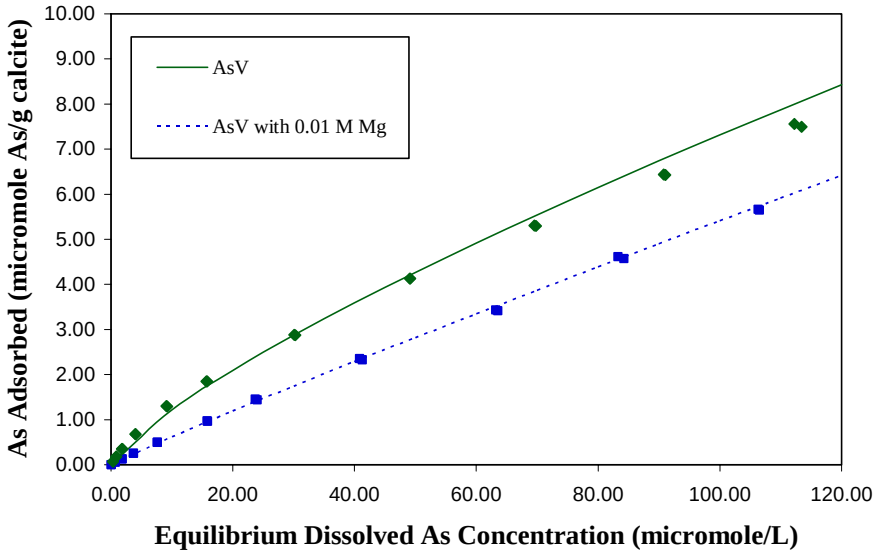

Figure 37. Adsorption isotherms for $iAs^{V}$and iAs^{V} with 0.01 M Mg^{2+} with experimental data points, and the model fit represented by the curve.

1.000 and shows that the curve is close to linear across the range of equilibrium concentrations. The K_f values for the models represent the initial slopes of the curves at low equilibrium concentration. The lower K_f value for iAs^V with 0.01 M magnesium nitrate (0.1483) than that of iAs^V without added magnesium nitrate (0.2042) shows that added 0.01 M magnesium nitrate decreases the adsorption at low equilibrium concentrations and suggests that the added magnesium nitrate may have altered calcite surface properties that directly impact adsorption at low concentrations.

Adsorption of Phosphate on Calcite. The adsorption of phosphate, P, on calcite was described using both the Freundlich and Langmuir models, and the plots of the models and experimental data are represented in Figure 38. The adsorption of phosphate

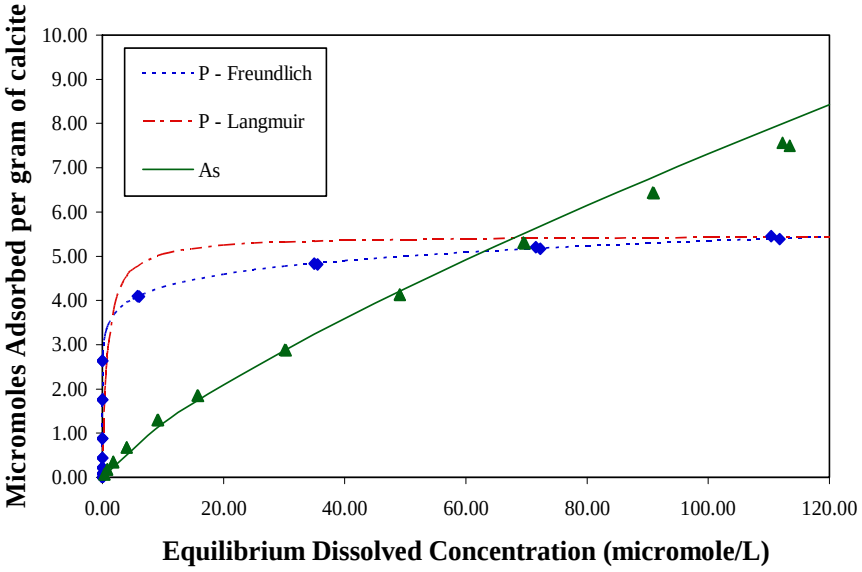

Figure 38. Adsorption isotherms for P and iAs^V with experimental data points and the P-Langmuir and Freundlich models represented by the curves.

on calcite is very different than the previously evaluated adsorption of arsenic on calcite and shows strong adsorption with a tendency towards an adsorption maximum. This behavior is more conducive to the Langmuir model than was observed with the previous isotherms. The Freundlich parameters are given in Table 5 and the Langmuir parameters are given in Table 6. The K_f value for the phosphate model is 3.47 and represents greater initial adsorption by an order of magnitude than that of any arsenic species evaluated in this study. The Langmuir model binding constant, K_L, for phosphate (1.24) as compared to the binding constant for iAs^V (0.0160) also demonstrates this adsorption behavior. The adsorption maximum (b) is 5.4645 and represents an estimate of the maximum amount of phosphate (µmoles) that could be adsorbed per gram of calcite. The Freundlich model coefficient of determination (R^2 of 0.999) compared to that of the Langmuir model (R^2 of 0.997) demonstrates that the Freundlich model continues to provide slightly better estimates of the experimental data.

Evaluation of Chemical Equilibrium Using MINTEQA2

Modeling Calcite Equilibrium. The MINTEQA2 model was used to calculate the molar concentrations and activities of dissolved aqueous species and phase distribution of calcite at equilibrium based on the amount of calcite added to the suspension. The amount of calcite (0.2 mol L^{-1}) added as the initial solid phase, and the equilibrium pH (7.95) were the only parameters used for the model. The phase distribution of the added calcite at equilibrium was shown to be 99.4% solid phase and 0.6% aqueous phase. MINTEQA2 calculated the ionic strength in solution to be 2.78×10^{-03}, and this value was used to determine the activities and concentrations of species in solution. The two

primary species listed in the dissolved aqueous phase were Ca^{2+} and HCO_3^- and had concentrations of 1.11 x 10^{-03} M and 1.08 x 10^{-03} M, respectively.

Modeling Phosphate Solubility. The MINTEQA2 speciation program was used to calculate the saturation state with respect to possible calcium phosphate solid phases based on the laboratory measurements of the aqueous phase composition at equilibrium. Analysis for calcium, alkalinity, pH and phosphate were performed and entered as model

Table 7. Species concentrations used for MINTEQA2 equilibrium calculations.

Molecular Species	Initial Concentration	Equilibrium Concentration
Ca^{2+}	†	4.8 x 10^{-04} M
HCO_3^-	†	1.6 meq L^{-1}
P (low)	8.7 x 10^{-05} M	5.8 x 10^{-06} M
P (high)	2.6 x 10^{-04} M	1.5 x 10^{-04} M
iAs^V (low)	8.8 x 10^{-06} M	3.3 x 10^{-07} M
iAs^V (high)	2.6 x 10^{-04} M	1.1 x 10^{-04} M

† Not determined

parameters. Solids were not allowed to precipitate so that the model equilibrium output would generate the species equilibrium concentrations from dissolved component concentrations that were measured in the laboratory. The experimental pH was 7.95. The initial and equilibrium concentrations of Ca^{2+}, HCO_3^-, and P at low and high P conditions are listed in Table 7. The model output for the sample with a low initial dissolved phosphate concentration indicated saturation indices for the solid phases as listed in Table 8. The model output for the sample with a high initial dissolved phosphate concentration indicated saturation indices for the solid phases as listed in Table 9.

Table 8. Saturation indices for calcium solid phases with a low initial dissolved phosphate concentration.

Calcium Solid Phases	SI
Calcite	-0.140
$CaHPO_4 \cdot 2\ H_2O$	-2.232
$Ca_5(PO_4)_3(OH)$	5.632
$CaHPO_4$	-1.952
$Ca_3(PO_4)_2$ (beta)	-1.044
$Ca_4H(PO_4)_3 \cdot 3\ H_2O$	-4.112

Table 9. Saturation indices for calcium solid phases with a high initial dissolved phosphate concentration.

Calcium Solid Phases	SI
Calcite	-0.248
$CaHPO_4 \cdot 2\ H_2O$	-0.832
$Ca_5(PO_4)_3(OH)$	9.792
$CaHPO_4$	-0.552
$Ca_3(PO_4)_2$ (beta)	1.736
$Ca_4H(PO_4)_3 \cdot 3\ H_2O$	0.069

At the low initial dissolved phosphate concentration, the MINTEQA2 model output of possible calcium phosphate solid phases indicated that the experimental system was not in equilibrium with respect to any of these hypothetical solid phases. At the high initial dissolved phosphate concentration, the MINTEQA2 model output of possible calcium phosphate solid phases showed $Ca_4H(PO_4)_3 \cdot 3\ H_2O$ to be the most likely solid phase controlling phosphate solubility. Based on previous studies by Tunesi et al. (1999), the most likely calcium phosphate solid phase to form at these experimental conditions is $Ca_5(PO_4)_3(OH)$, hydroxyapatite, although they suggested that hydroxyapatite does not

precipitate from solution until a millimolar concentration of Ca^{2+} and phosphate has been reached. In these experiments, it could be likely that surface adsorption of phosphate, as opposed to solid phase precipitation of calcium phosphate, at both low and high concentration is the primary mechanism of phosphate adsorption.

Editing the Thermodynamic Database for Arsenic Solubility. Equilibrium constants for dissolved arsenate and calcium arsenate species were taken from the study by Bothe and Brown (1999b) and added to the MINTEQA2 thermodynamic database.

Table 10. Equilibrium constants for dissolved aqueous species added and edited in the MINTEQA2 thermodynamic database.

Reaction	Log K†	Temperature
$AsO_4^{3-} + H^+ \Leftrightarrow HAsO_4^{2-}$	11.602	25 °C
$HAsO_4^{2-} + H^+ \Leftrightarrow H_2AsO_4^-$	6.761	25 °C
$H_2AsO_4^- + H^+ \Leftrightarrow H_3AsO_4$	2.249	25 °C
$Ca^{2+} + AsO_4^{3-} \Leftrightarrow CaAsO_4^-$	4.36	23 °C
$Ca^{2+} + HAsO_4^{2-} \Leftrightarrow CaHAsO_4^o$	2.66	23 °C
$Ca^{2+} + H_2AsO_4^- \Leftrightarrow CaH_2AsO_4^+$	1.30	23 °C

† Bothe and Brown, 1999b

Table 11. Solubility products for calcium arsenate solid phases added to the MINTEQA2 thermodynamic database.

Calcium Arsenate Hydrate	pKsp†
$Ca_4(OH)_2(AsO_4)_2 \cdot 4\ H_2O$	29.20
$Ca_5(AsO_4)_3OH$	38.04
$Ca_3(AsO_4)_2 \cdot 3^2/_3\ H_2O$	21.00
$Ca_3(AsO_4)_2 \cdot 4^1/_4\ H_2O$	21.00
$Ca_5H_2(AsO_4)_4 \cdot 9\ H_2O$	31.49
$CaHAsO_4 \cdot H_2O$	4.79

† Bothe and Brown, 1999b

The calcium arsenate and arsenic acid reactions, with log K values and temperatures, are given in Table 10. The solubility products (pK_{sp}) of calcium arsenate solid phases as determined by Bothe and Brown (1999b) were added to the MINTEQA2 thermodynamic database and are listed in Table 11.

Modeling Arsenic Solubility. The MINTEQA2 speciation program was used to calculate the saturation state with respect to possible calcium arsenate hydrate solid phases (listed in Table 11) based on the laboratory measurements of the aqueous phase composition at equilibrium. Analysis for calcium, alkalinity, pH and arsenic were performed and input as model parameters. Solids were not allowed to precipitate so that the model equilibrium output would generate the species equilibrium concentrations from dissolved component concentrations that were measured in the laboratory. The experimental pH was 7.95. The initial and equilibrium concentrations of Ca^{2+}, HCO_3^-, and iAs^V at low and high iAs^V conditions are listed in Table 7. The model output for the sample with a low initial dissolved arsenic concentration indicated saturation indices for the solid phases as listed in Table 12. The model output for the sample with a high initial

Table 12. Saturation indices for calcium solid phases with a low initial dissolved arsenic concentration.

Calcium Solid Phases	SI
Calcite	-0.138
$Ca_4(OH)_2(AsO_4)_2 \cdot 4\ H_2O$	16.553
$Ca_5(AsO_4)_3OH$	6.579
$Ca_3(AsO_4)_2 \cdot 3\ ^2/_3\ H_2O$	-4.138
$Ca_3(AsO_4)_2 \cdot 4\ ^1/_4\ H_2O$	-4.138
$Ca_5H_2(AsO_4)_4 \cdot 9\ H_2O$	-31.276
$CaHAsO_4 \cdot H_2O$	-14.024

Table 13. Saturation indices for calcium solid phases with a high initial dissolved arsenic concentration.

Calcium Solid Phases	SI
Calcite	-0.248
$Ca_4(OH)_2(AsO_4)_2 \cdot 4\ H_2O$	21.399
$Ca_5(AsO_4)_3OH$	13.959
$Ca_3(AsO_4)_2 \cdot 3\ ^2/_3\ H_2O$	0.819
$Ca_3(AsO_4)_2 \cdot 4\ ^1/_4\ H_2O$	0.819
$Ca_5H_2(AsO_4)_4 \cdot 9\ H_2O$	-21.251
$CaHAsO_4 \cdot H_2O$	-11.490

dissolved arsenic concentration indicated saturation indices for the solid phases as listed in Table 13.

At the low initial dissolved iAs^V concentration, the MINTEQA2 model output of possible calcium arsenate solid phases did not indicate that any solid phase was in equilibrium with the experimental system. At the high initial dissolved iAs^V concentration, the MINTEQA2 model output of possible calcium arsenate solid phases indicated that $Ca_3(AsO_4)_2 \cdot 3\ ^2/_3\ H_2O$ and $Ca_3(AsO_4)_2 \cdot 4\ ^1/_4\ H_2O$ are the most likely solid phases controlling arsenate solubility.

These results are consistent with those reported by Bothe and Brown (1999a) who synthesized calcium arsenate hydrates by the reaction of $Ca(OH)_2$ and H_3AsO_4 and characterized the molecular structure of the solid phases by X-ray diffraction. In the study, it was shown that $Ca_3(AsO_4)_2 \cdot 3\ ^2/_3\ H_2O$, $Ca_3(AsO_4)_2 \cdot 4\ ^1/_4\ H_2O$ and $Ca_5(AsO_4)_3OH$ are the primary solid phases formed at Ca/As ratios between 1.5 and 1.9, although only $Ca_3(AsO_4)_2 \cdot 4\ ^1/_4\ H_2O$ formed at pH less than 9. The $Ca_5(AsO_4)_3OH$ solid phase was also found to be present at these reaction conditions but only in minor

amounts. The initial Ca/As ratio of 1.8 and the pH of 7.95, at a high initial dissolved arsenic concentration, suggests that $Ca_3(AsO_4)_2 \cdot 4\ ^1/_4\ H_2O$ is the most likely solid phase controlling arsenate solubility. Although, these results indicate that the calcium arsenate solid phase, $Ca_3(AsO_4)_2 \cdot 4\ ^1/_4\ H_2O$, could be controlling arsenic solubility by surface precipitation, further studies will be needed to determine that surface adsorption is not the primary mechanism of arsenate adsorption across the range of concentrations evaluated in this study.

CONCLUSIONS

Arsenic adsorption and mobility in geochemical systems is impacted by mineralogical and environmental factors. Calcite is an important mineral constituent that can exert a major influence on a system's physical and chemical characteristics. The partitioning of arsenic between solid and aqueous phases in the environment can be directly impacted by its interaction with calcite. The results of this research show that adsorption and retention of arsenic to the surface of calcite can be significant at the concentrations evaluated in this study.

In the current study, calcite particle size, as evaluated by scanning electron microscopy, was smaller than that determined by laser-diffraction particle-size analysis. The assay of contaminants in calcite could be an important factor that affects particle aggregation and the results of these analyses. The trace elemental content of the calcite lots used in this study suggests that sulfate content might have impacted the affinity of calcite particles to bond together and form aggregates. Previous studies (Celi et al., 2000) have shown the impact of anion adsorption to the surface of calcite and its impact on particle-size distribution and aggregate stability. Tung et al. (2004) used scanning electron microscopy images to show the increased aggregation of calcite particles due to the inclusion of sulfate. The consequences of this phenomenon should be considered when assessing calcite particle-size distribution using laser diffraction. Techniques, such as the Brunauer-Emmett-Teller (BET) method which assesses surface area, should be employed to provide a more comprehensive understanding of calcite surface properties which directly affect the study of contaminant surface adsorption. Previous characterization by Lee et al. (2005) on this Alfa Aesar reagent grade calcite (calcite lot

A, used for the adsorption studies) provided a surface area measurement (0.2 m^2/g) from which a qualitative interpretation of the results can be made.

The kinetic evaluation in this study has shown that the adsorption of iAs^V to calcite is a comparatively fast reaction within the first hour followed by a slower and relatively constant reaction rate until equilibrium is achieved. The change in reaction rate might be indicative of a change in the mechanism of bonding although Veith and Sposito (1977) demonstrated that reaction mechanisms cannot be inferred from adsorption studies alone. Techniques such as X-ray absorption fine structure spectroscopy (XAFS) could elucidate atomic-scale information such as bond distances and orbital symmetries of the calcite-arsenic bonds and infer mechanistic changes associated with a change in the reaction kinetics. The kinetics assessment performed was also important to establish the reaction time necessary to achieve equilibrium. The kinetic experiments at high and low concentrations of arsenic showed that equilibrium was established within approximately 8 hours and thus supported the use of 24-hour equilibration times during experiments.

The effect of oxidation state on the adsorption of arsenic to calcite was significant and suggested that a reduced environmental system, which would favor iAs^{III}, could lower the amount of arsenic adsorbed to the surface of calcite. A reduced system with high pCO_2 and low pO_2 could result in increased arsenic mobility when calcite is the dominant mineral impacting arsenic adsorption.

The methylation of arsenic also had an effect on the adsorption behavior. The methylated forms of arsenic were sorbed to a lesser degree that either inorganic form of arsenic. This comparative adsorption behavior could have important implications when considering the biomethylation of arsenic in the environment. Increased arsenic mobility

could result in higher bioavailability and have adverse implications to agriculture and human health. This study also showed that DMA^V adsorption was greater than MMA^V adsorption, suggesting that the increase in methylation from MMA^V to DMA^V could favor a slightly reduced mobility of arsenic in the environment due to adsorption and retention by calcite.

The effects of some environmentally important groundwater species on arsenic adsorption to calcite were also studied in this research. Dissolved calcium resulted in increased adsorption of iAs^V when at a low concentration of 0.01 M. This phenomenon could be due to the impact of adsorbed Ca^{2+} on the surface properties of calcite, which could result in a mineral surface with higher positive charge and greater propensity for the adsorption of negatively charged species of arsenic. Further increases in $Ca(NO_3)_2$ concentration resulted in a decrease in iAs^V adsorption. This result indicates that NO_3^{3-} might have been competing with iAs^V for adsorption to calcite surface sites. Also, higher ionic strengths might result in greater solubility of calcium arsenate solid phases. Dissolved Mg^{2+}, at a concentration of 0.01 M $Mg(NO_3)_2$, reduced the adsorption of iAs^V to calcite, suggesting that Mg^{2+} might have affected the calcite surface in such a manner that it resulted in reduced interaction of iAs^V with calcite. Millero et al. (2001) suggested that the decreased adsorption of phosphate by calcite might have been related to the interaction of phosphate with dissolved magnesium. In this study, the adsorption of inorganic and methylated forms of arsenic by calcite was considerably less than that of phosphate. The difference in adsorption behaviors of arsenic and phosphate likely indicate different adsorption mechanisms, although further spectroscopic studies are needed to elucidate the mechanism of arsenic adsorption by calcite. In previous studies

by Celi et al. (2000) on the adsorption of phosphate to calcite, it was suggested that a change in mechanism from surface adsorption to surface precipitation of phosphate by calcite occurred at equilibrium phosphate concentrations in the millimolar range. The reactions of phosphate at the concentrations evaluated in this study should be predominantly due to surface adsorption by calcite. The high degree of phosphate adsorption by calcite could have very important implications on arsenic mobility in soil and groundwater since phosphate was shown to be preferentially adsorbed by calcite at all concentrations. Above equimolar dissolved arsenic and phosphate concentrations of 90 µM, the adsorption of iAs^V by calcite was completely inhibited by phosphate. Tunesi et al. (1999) suggested that calcite provides a surface for the specific adsorption of phosphate at low concentrations.

Arsenic adsorption by calcite was effectively described by the empirical, Freundlich equation. The Langmuir equation was not as useful and did not effectively predict arsenic adsorption by calcite since clear experimental adsorption maxima were not observed. Phosphate adsorption behavior was distinctly different from that of arsenic and was effectively described using the Langmuir equation.

MINTEQA2 equilibrium results at a low initial dissolved phosphate concentration indicated that an adsorption reaction might be controlling phosphate solubility. Results at a high initial dissolved phosphate concentration suggested that $Ca_4H(PO_4)_3 \cdot 3\ H_2O$ could possibly be controlling phosphate equilibrium, although previous studies (Tunesi et al., 1999) have suggested that surface adsorption of phosphate by calcite should be predominant at the high initial phosphate concentration evaluated in this study. Spectroscopic evaluation would be needed to definitively assess whether

$Ca_4H(PO_4)_3 \cdot 3\ H_2O$ precipitated at the surface of calcite. Equilibrium calculations using MINTEQA2 indicated that adsorption reactions might be controlling arsenic solubility at a low initial iAs^V concentration. At a high initial iAs^V concentration, MINTEQA2 equilibrium calculations indicated that $Ca_3(AsO_4)_2 \cdot 3\ ^2/_3\ H_2O$ and $Ca_3(AsO_4)_2 \cdot 4\ ^1/_4\ H_2O$ solid phases are possibly controlling arsenic solubility in these experiments. The $Ca_3(AsO_4)_2 \cdot 4\ ^1/_4\ H_2O$ solid phase control of arsenic solubility was consistent with those presented by Bothe and Brown (1999a) based on the initial Ca/As ratio and pH in this study.

In environmental systems with a high abundance of calcite, the adsorption and transport of arsenic is impacted by its interaction with dissolved aqueous calcium and solid phase calcite. In previous studies by Goldberg and Glaubig (1988), the adsorption of arsenic in a calcareous, montmorillonitic soil was shown to be significantly reduced by the removal of calcite. This study suggests that adsorption and retention of arsenic by calcite can be significant. Further research that assesses the adsorption of arsenic by calcite and other soil constituents is greatly needed. Previous studies (e.g., Lafferty and Loeppert, 2005) have suggested that Fe and Al oxides might also have a significant impact on the control of arsenic in soil adsorption processes. A more holistic approach that uses complex mineral assemblages of calcite, Fe and Al oxides, and other soil constituents could further distinguish the effect of the relative abundance of each constituent on the adsorption behavior of arsenic in geochemical systems.

REFERENCES

Allison, J. D., D. S. Brown, and K. J. Novo-Gradac. 1991. MINTEQA2. A geochemical assessment model for environmental systems. U. S. Environmental Protection Agency. Athens, GA.

Amer, F., A. A. Mahmoud, and V. Sabet. 1985. Zeta potential and surface area of calcium carbonate as related to phosphate sorption. Soil Sci. Soc. Am. J. 49: 1137 – 1142.

Bentley, R., and T. Chasteen. 2002. Microbial methylation of metalloids: Arsenic, antimony, and bismuth. Microbiol. Mol. Biol. Rev. 66: 2, 250 – 271.

Bissen, M., and F. H. Frimmel. 2003. Arsenic – A review. Part 1: Occurrence, toxicity, speciation, and mobility. Acta Hydrochim. Hydrobiol. 31: 1, 9 – 18.

Bothe, Jr., James V., and Paul W. Brown. 1999a. Arsenic immobilization by calcium arsenate formation. Environ. Sci. Technol. 33: 3806 – 3811.

Bothe, Jr., James V., and Paul W. Brown. 1999b. The stabilities of calcium arsenates at 23 $\pm$ 1^{o} C. Journal of Hazardous Materials. B69: 197 – 207.

Brady, Nyle C., and Ray R. Weil. 2002. The nature and property of soils. 13th ed. Pearson Education Inc., Upper Saddle River, NJ.

Celi, L., S. Lamaccia, and E. Barberis. 2000. Interaction of inositol phosphate with calcite. Nutrient Cycling in Agroecosystems 57: 271 – 277.

Cheng, Likwan, Paul Fenter, Neil Sturchio, Zhong Zhong, and Michael Bedzyk. 1999. X-ray standing wave study of arsenite incorporation at the calcite surface. Geochimica et Cosmochimica Acta. 63: 19/20, 3153 – 3157.

Choquette, P. W., and L. C. Pray. 1970. Geological nomenclature and classification of porosity in sedimentary carbonates. American Association of Petroleum Geologists Bulletin. 54: 207 – 250.

Cotton, F. A., and Geoffrey Wilkinson. 1976. Basic inorganic chemistry. John Wiley and Sons, New York.

Dombrowski, Paul M., W. Long, K. Farley, J. D. Mahony, J. F. Capitani, and D. M. DiToro. 2005. Thermodynamic analysis of arsenic methylation. Environ. Sci. Technol. 39: 2169 – 2176.

Doner, H. E., and W. C. Lynn. 1989. Carbonate, halide, sulfate, and sulfide minerals. Soil Sci. Soc. Am. Book Series: 1. 6: 279 – 330.

Doner, H. E., and P. R.. Grossl. 2002. Carbonates and evaporites. Soil Sci. Soc. Am. Book Series: 7. 6: 199 – 228.

Dunham, R. J. 1962. Classification of carbonate rocks according to depositional texture. American Association of Petroleum Geologists Memoir. 1: 108 – 121.

Dutre, Veronika, and Carlo Vandecasteele. 1998. Immobilization mechanism of arsenic in waste solidified using cement and lime. Environ. Sci. Technol. 32: 2782 – 2787.

Elzinga, E.J., and R. J. Reeder. 2002. X-ray absorption spectroscopy and study of Cu2+ and Zn2+ absorption complexes at the calcite surface: Implications for site specific metal incorporation preferences during calcite crystal growth. Geochim. Cosmochim. Acta. 66: 3943 – 3954.

Embry, A. F. and J. E. Klovan. 1971. A late Devonian reef tract on northeastern Banks Island, NWT. Bulletin of Canadian Petroleum Geology. 19: 730 – 781.

Eshel, G., G. J. Levy, U. Mingelgrin, and M. J. Singer. 2004. Critical evaluation of the use of laser diffraction for particle-size distribution analysis. Soil Sci. Soc. Am. J. 68: 736 – 743.

Essington, Michael E., 2003. Soil and water chemistry: An integrative approach. CRC Press, Inc., Boca Raton, FL.

Fenter P., P. Geissbuhler, E. DiMasi, G. Srajer, L. B. Sorensen, and N. C. Sturchio. 1999. Surface speciation of calcite observed in situ by high-resolution x-ray reflectivity. Geochimica et Cosmochimica Acta. 64: 7, 1221 - 1228.

Freundlich, Herbert. 1926. Colloid and capillary chemistry. Methuen, London.

Garrels, R.M., and M. E. Thompson. 1962. A chemical model for sea water at 25^{o}C and one atmosphere total pressure. Amer. J. Sci. 260: 57 – 66.

Goldberg, S., and R. A. Glaubig. 1988. Anion sorption on a calcareous, montmorillonitic soil – arsenic. Soil Sci. Soc. Am. J. 52: 1297 – 1300.

Goldelitsas, A., J. M. Astilleros, K. Hallam, S. Harissopoulos, and A. Putnis. 2003. Interaction of calcium carbonates with lead in aqueous solution. Environ. Sci. Technol. 37: 3351 – 3360.

Ham, W. E. and L. C. Pray. 1962. Modern concepts and classifications of carbonate rocks. American Association of Petroleum Geologists Memoir. 1: 2 – 19.

Lafferty, B., and R. Loeppert. 2005. Methyl arsenic adsorption and desorption behavior on iron oxides. Environ. Sci. Technol. 39: 2120 – 2127.

Langmuir, D. 1997. Aqueous environmental geochemistry. Prentice-Hall Inc., Upper Saddle River, NJ.

Langmuir, I., 1918. The adsorption of gases on plane surfaces of glass, mica, and platinum. J. Am. Chem. Soc. 40: 1361.

Lee, Young J., Evert J. Elzinga, and Richard J. Reeder. 2005. Cu(II) adsorption at the calcite-water interface in the presence of natural organic matter: Kinetic studies and molecular-scale characterization. Geochim. Cosmochim. Acta. 69: 1, 49 – 61.

Le Guern, C., P. Baranger, C. Crouzet, F. Bodenan, and P. Conil. 2003. Arsenic trapping by iron oxyhydroxides and carbonates at hydrothermal spring outlets. Appl. Geochem. 18: 1313 – 1323.

Lindsay, W. L. 1979. Chemical equilibria in soils. Wiley-Interscience, New York.

Magalhaes, M. Clara F. 2002. Arsenic. An environmental problem limited by solubility. Pure Appl. Chem. 74: 1843 – 1850.

Martin-Garin A., J. P. Gaudet, L. Charlet, X. Vitart. 2002. A dynamic study of the sorption and the transport processes of cadmium in calcareous sandy soils. Waste Manag. 2: 22, 201 - 7.

Matar, A., J. Torrent, and J. Ryan. 1992. Soil and fertilizer phosphorus and crop response in dryland Mediterranean zone. Adv. Soil Sci. 18: 81 – 146.

McMurray, John. 1984. Organic chemistry. Brooks/Cole Publishing Company, Monterey, CA.

Millero, Frank, Fen Huang, Xiaorong Zhu, Xuewu Liu, and Zia-Zhong Zhang. 2001. Adsorption and desorption of phosphate on calcite and aragonite in seawater. Aquatic Geochemistry 7: 33 – 56.

Mishra S.K. 1978. The electrokinetics of apatite and calcite in inorganic electrolyte environment. International Journal of Mineral Processing. 5: 69 – 83.

Ohki, A., K. Nakayachigo, K. Naka, and S. Maeda. 1996. Adsorption of inorganic and organic arsenic compounds by aluminum-loaded coral limestone. Applied Organometallic Chemistry. 10: 747 – 752.

Ott, R. Lyman, and Michael Longnecker. 2001. An introduction to statistical methods and data analysis. 5th edition. Duxbury, Pacific Grove, CA.

Paquette J., and R. Reeder. 1995. Relationship between surface structure, growth mechanism, and trace element incorporation in calcite. Geochimica et Cosmochimica Acta. 59: 4, 735 – 749.

Reeder, Richard. 1996. Interaction of divalent cobalt, zinc, cadmium and barium with the calcite surface during layer growth. Geochim. Cosmochim. Acta. 60: 9, 1543 – 1552.

Romero, F. M., M. A. Armienta, and A. Carillo-Chavez. 2004. Arsenic sorption by carbonate rich aquifer material, a control of arsenic mobility at Zimapan, Mexico. Arch. Environ. Contam. Toxicol. 47: 1 – 13.

Safe Drinking Water Act (SDWA). U.S. Code: Title 42, chapter 6A, subchapter XII, part B, section 300g – 1, (1974).

Smith, R. M., and A. E. Martell. 1976. Critical stability constants. IV. Inorganic complexes. Plenum Press, New York.

Song, S., A. Lopez-Valdivieso, D. J. Hernandez-Campos, C. Peng, M. G. Monroy-Fernandez, and I. Razo-Soto. 2006. Arsenic removal from high-arsenic water by enhanced coagulation with ferric ions and course calcite. Water Research. 40: 364 – 372.

Staudt, W. J., R. J. Reeder and M. A. A. Schoonen. 1994. Surface structural controls on compositional zoning of SO_4^{2-} and SeO_4^{2-} in synthetic calcite single crystals. Geochim. Cosmochim. Acta. 58: 9, 2087 – 2098.

Stipp, S., and M. Hochella. 1991. Structure and bonding environments at the calcite surface as observed with x-ray photoelectron microscopy (XPS) and low energy electron diffraction (LEED). Geochimica et Cosmochimica Acta. 55: 1723 – 1736.

Tung, Nguyen Phuong, Nguyen Thi Phuong Phong and Nguyen Hoang Duy. 2004. The use of scanning electron microscopy (SEM) investigating scale inhibition in seawater and scale morphology. Proceedings of the Ninth Asia Pacific Physics Conference (9^{th} APPC), Hanoi, Vietnam. Institute of Materials Science, Ho Chi Minh City, Vietnam.

Tunesi, Simonetta, Valerie Poggi and Carlo Gessa. 1999. Phosphate adsorption and precipitation in calcareous soils: The role of calcium ions in solution and carbonate minerals. Nutrient Cycling in Agroecosystems. 53: 219 – 227.

U.S. Environmental Protection Agency. 1982. An exposure and risk assessment for arsenic. Office of Water Regulations and Standards. 440: 4-85-005.

Van Cappellen, P., L. Charlet, W. Stumm and P. Wersin. 1993. A surface complexation model of the carbonate mineral-aqueous solution interface. Geochimica et Cosmochimica Acta. 57: 3505 – 3518.

Vasken, Aposhian H. 1997. Enzymatic methylation of arsenic species and other new approaches to arsenic toxicity. Annual Review of Pharmacology and Toxicology. 37: 397 – 419.

Veith, J. A., and Garrison Sposito. 1977. On the use of the langmuir equation in the interpretation of “adsorption” phenomena. Soil Sci. Soc. Am. J. 41: 697 – 702.

Wagman, D. D., H. H. Evans, V. B. Parker, R. H. Schumm, I. Harlow, S. M. Bailey, K. L. Churney, and R. L. J. Butall. 1982. The NBS tables of chemical thermodynamic properties – selected values for inorganic and C-1 and C-2 organic-substances in SI units. J. Phys. Chem. Ref. Data. 11: 392.

Zhu, Y. N., X. H. Zhang, Q. L. Xie, D. Q. Wang, and G. W. Cheng. 2006. Solubility and stability of calcium arsenates at 25^{o}C. Water, Air and Soil Pollution. 169: 221 – 238.

VITA

Name: Robert Garret Jones

Address: 8806 Amblewood Dr., Houston, TX 77099

Email Address: RGJoneser@yahoo.com

Education: B.S., Chemistry, Texas A&M University, 1988.

M.S., Soil Science, Texas A&M University, 2007.

Experience: After graduation from Texas A&M in 1988, Mr. Jones continued with graduate studies in chemistry at the University of Houston and performed laser-induced, fluorescence spectroscopy research. Mr. Jones later accepted a position at the Browning-Ferris Industries, National Environmental Laboratory, and worked within the inorganic chemistry division. He also worked as a senior chemist and laboratory supervisor at the Griffin Corporation chemical manufacturing facility in Houston, Texas where he served on the process improvement and safety committees and was instrumental in leading on issues concerning process control and wastewater management. During this time, he was also given a special interim assignment at the corporate facility in Georgia as a laboratory manager. Mr. Jones subsequently accepted a project manager position with Xenco Laboratories in Houston, Texas and was later promoted to laboratory manager of the Dallas, Texas facility. After his tenure with Xenco, Mr. Jones accepted a position with the Office of the Texas State Chemist in College Station, Texas and was accepted into the Soil Science graduate program at Texas A&M University.